Asymptotic normalization coefficients and continuum coupling in mirror nuclei

J. Okołowicz, N. Michel, W. Nazarewicz, and M. Płoszajczak

Phys. Rev. C **85**, 064320 — Published 21 June 2012

DOI: 10.1103/PhysRevC.85.064320

Asymptotic normalization coefficients and continuum coupling in mirror nuclei

J. Okołowicz,[1] N. Michel,[2,3] W. Nazarewicz,[3,4,5] and M. Płoszajczak[6]

[1] *Institute of Nuclear Physics, Polish Academy of Sciences, Radzikowskiego 152, PL-31342 Kraków, Poland*
[2] *Department of Physics, Post Office Box 35 (YFL), University of Jyväskylä, FI-40014 Jyväskylä, Finland*
[3] *Department of Physics and Astronomy, University of Tennessee, Knoxville, Tennessee 37996, USA*
[4] *Physics Division, Oak Ridge National Laboratory, Oak Ridge, Tennessee 37831, USA*
[5] *Institute of Theoretical Physics, University of Warsaw, ul. Hoża 69, PL-00-681 Warsaw, Poland*
[6] *Grand Accélérateur National d'Ions Lourds (GANIL), CEA/DSM - CNRS/IN2P3, BP 55027, F-14076 Caen Cedex, France*

(Dated: June 5, 2012)

Background: An asymptotic normalization coefficient (ANC) characterizes the asymptotic form of a one-nucleon overlap integral required for description of nucleon-removal reactions.

Purpose: We investigate the impact of the particle continuum on proton and neutron ANCs for mirror systems from *p*- and *sd*-shell regions.

Method: We use the real-energy and complex-energy continuum shell model approaches.

Results: We studied the general structure of the single-particle ANCs as a function of the binding energy and orbital angular momentum. We computed ANCs in mirror nuclei for different physical situations, including capture reactions to weakly-bound and unbound states.

Conclusions: We demonstrated that the single-particle ANCs exhibit generic behavior that is different for charged and neutral particles. We verified the previously proposed relation [1] between proton and neutron mirror ANCs. We find minor modifications if the spectroscopic strength is either localized in a single state or broadly distributed. For cases when several states couple strongly to the decay channel, these modifications may reach 30%.

PACS numbers: 21.10.Jx, 21.10.Sf, 21.60.Cs, 24.10.Cn

I. INTRODUCTION

The ANC method [2] has proved useful as an indirect tool to determine direct capture reaction rates [3–5] both to well-bound and weakly-bound states. The ANC of the virtual proton decay of a nucleus $a \to b + p$ is related to the astrophysical S-factor for a proton capture reaction $b(p,\gamma)a$ at stellar energies, and can be obtained in transfer reactions that offer higher cross-sections; hence, it provides an alternative to direct reactions at relevant energies in astrophysical processes [3, 5, 6]. The method depends on the peripheral nature of low-energy capture reactions, in which case the cross-section is determined by the tail of the radial overlap integral between the wave functions of the final nucleus and initial colliding systems.

The ANC, or the nuclear vertex constant, for the decay $a \to b + c$ is proportional to the asymptotic behavior of the wave function representing the relative motion of particles b and c. This quantity is closely related to the reaction amplitude [5] and – unlike the spectroscopic factor – is invariant under finite-range unitary transformations of the nucleon-nucleon (NN) interaction [7]; hence is less dependent on the choice of a short-range potential.

Recently, it has been advocated [1] that the charge symmetry of the nuclear force could be used to relate the ANC of the proton decay to the virtual neutron decay of the mirror nucleus. This observation opens an attractive possibility to learn about the decay width of hardly accessible states in proton-rich nuclei from transfer reaction studies in mirror-bound systems using stable beams. It remains, however, an important question to what extent the charge symmetry argument is sufficient to extract reliable information about the width of an unbound state of some nucleus from the ANC in its bound mirror partner. It is well-known, for example, that threshold effects lead to striking differences in the energy spectra of mirror nuclei having different particle emission thresholds [8]. Indeed, for near-threshold states, the configuration mixing involving scattering states strongly depends on the positions of particle emission thresholds in mirror systems (the binding energy effect) [9], and on different asymptotic behavior of neutron and proton wave functions. The latter effect leads to the universal behavior of cross sections [10, 11] and overlap integrals [12–14] in the vicinity of the reaction threshold.

The main objective of this study is to verify the conjecture of Refs. [1, 15–18] that the ratio $\mathcal{R}$ of ANCs for mirror pairs is both approach-independent and interaction-independent. To investigate the proposed link between proton and neutron mirror ANCs [1], we employ the framework of the nuclear Shell Model (SM) for open quantum systems (OQS), i.e., the continuum shell model (CSM) [19, 20], which offers a realistic treatment of the configuration mixing in well-bound, weakly-bound, and unbound states.

The paper is organized as follows. In Sec. II we discuss basic features of ANCs. In particular, we review properties of ANCs for proton wave functions in bound nuclei

and the limiting behavior of ANCs for charged particles and neutrons. The CSM results for the ANC in mirror p- and (sd)-shell nuclei are discussed in Sec. III. We employ the complex-energy Gamow Shell Model (GSM) and the real-energy Shell Model Embedded in the Continuum (SMEC) to describe ANCs for bound states and resonances. We also analyze the dependence of the ANCs in mirror systems, and their ratios, on the strength of the continuum coupling and configuration mixing. Finally, Sec. IV summarizes the results of our work.

II. BASIC FEATURES OF THE ASYMPTOTIC NORMALIZATION COEFFICIENT

Let us consider the radiative capture reaction $b + c \to a + \gamma$, and define the radial overlap function I^a_{bc} for a process $a \to b + c$. In the asymptotic region, I^a_{bc} can be written as:

$$I^a_{bc;\ell j}(r) \sim \frac{1}{r} C_{\ell j} W_{-\eta,\ell+1/2}(2\kappa r), \tag{1}$$

where $W_{-\eta,\ell+1/2}$ is the Whittaker function and $C_{\ell j}$ is the ANC, a quantity characterizing the virtual decay of a nucleus into two particles b and c. In Eq. (1), r is the relative distance between b and c, $\kappa = \sqrt{2\mu S_c^{(a)}/\hbar^2}$ where $S_c^{(a)}$ is the separation energy of particle c in the nucleus a, and $\eta = Z_b Z_c e^2 \mu/\hbar^2\kappa$ where μ is the reduced mass of $b + c$. The quantum numbers ℓ and j are the orbital angular momentum and the channel angular momentum, respectively.

In this paper we shall assume that the particle c is a nucleon (proton or neutron); hence, $S_{n,p}^{(a)}$ is the one-nucleon separation energy. The corresponding radial overlap integral can be written as:

$$I^a_{bc;\ell j}(r) = \frac{1}{\sqrt{2J_a+1}} \sum_{\mathcal{B}} \langle \Psi_a^{J_a} || a^\dagger_{\ell j}(\mathcal{B}) || \Psi_b^{J_b} \rangle \langle r\ell j | u_{\mathcal{B}} \rangle, \tag{2}$$

where $a^+_{\ell j}(\mathcal{B})$ is a creation operator associated with the single-particle (s.p.) basis state $|u_{\mathcal{B}}\rangle$ and $\langle r\ell j|u_{\mathcal{B}}\rangle$ is the radial s.p. wave function. The sum in (2) runs over the complete s.p. basis. The squared norm of the radial overlap integral (2) defines the spectroscopic factor $S_{\ell j}$.

In the general case of multi-channel coupling, the ANC for a radiative capture reaction is defined in terms of the Hermitian norm $|C_\ell|$ of all the contributions corresponding to different couplings of the target state and the state in a parent nucleus:

$$|C_\ell| = \sqrt{\sum_j |C_{\ell j}|^2}. \tag{3}$$

For bound states, $I^a_{bc;\ell j}$ can be well approximated by the product of the spectroscopic amplitude $S^{1/2}_{\ell j}$ and the s.p. radial wave function $u_{\ell j}/r$ at a s.p. energy $-S_c^{(a)}$:

$$I^a_{bc;\ell j}(r) \sim \frac{1}{r} S^{1/2}_{\ell j} u_{\ell j}(r). \tag{4}$$

For $r \gg R$, where R is the nuclear radius, $u_{\ell j}$ is given by its asymptotic form

$$u_{\ell j}(r) = \beta_{\ell j} W_{-\eta,\ell+1/2}(2\kappa r), \tag{5}$$

where $\beta_{\ell j} = \beta_{\ell j}(S_c^{(a)})$ is the single-particle ANC (SPANC). Therefore, far from the region of nuclear interaction, $I^a_{bc;\ell j}$ behaves as:

$$I^a_{bc;\ell j}(r) \sim \frac{1}{r} S^{1/2}_{\ell j} \beta_{\ell j} W_{-\eta,\ell+1/2}(2\kappa r). \tag{6}$$

Hence, $\beta_{\ell j}$ is directly related to the ANC [21]:

$$C_{\ell j} = S^{1/2}_{\ell j} \beta_{\ell j}. \tag{7}$$

The relations (4)-(7) also hold for many-body resonances. Indeed, as demonstrated in GSM studies [12], the overlap function $I^a_{bc;\ell j}$ is well approximated by the product of the spectroscopic amplitude $S^{1/2}_{\ell j}$ and the s.p. resonance wave function of the average potential, which reproduces the Q-value of the reaction studied. Let us also recall that the astrophysical $\mathcal{S}_{bc}$-factor, in the limit of zero center-of-mass energy, $E_{\rm CM} = 0$, is simply proportional to $\beta^2_{\ell j}$ [3]:

$$\mathcal{S}_{bc}(0) \sim \beta^2_{\ell j} \equiv \beta^2_{\ell j}(\eta). \tag{8}$$

A. General properties of SPANCs for charged particles

In this section, we study the generic dependence of SPANCs on the separation energy, i.e., η. Let R_f ($R_f \gg R$) be the radius of the external region where the nuclear part of the potential is practically zero. In this region ($r \geq R_f$) the s.p. wave function $u_{\ell j}$ is given by Eq. (5), i.e., it is given by $W_{-\eta,\ell+1/2}(2\kappa r)$. For the normalized bound state, this implies that $\mathcal{N}_{\rm int} + \mathcal{N}_{\rm ext} = 1$, where $\mathcal{N}_{\rm int}$ is the norm of the internal part of the wave function, and

$$\mathcal{N}_{\rm ext} = \beta^2_{\ell j} \int_{R_f}^{+\infty} |W_{-\eta,\ell+1/2}(2\kappa r)|^2 \, dr \tag{9}$$

is the norm of the external part. Provided that the energy dependence of $\mathcal{N}_{\rm int}$ is weak (which is a reasonable assumption even if separation energy is close to zero), $\beta_{\ell j}$ should strongly depend on the value of the integral in Eq. (9).

In terms of the outgoing Coulomb wave function $H^+(\ell, \eta_k, kr)$, the Whittaker function can be written as

$$W_{-\eta,\ell+1/2}(2\kappa r) = H^+(\ell, \eta_k, kr) e^{i\frac{\pi\eta}{2} + i\frac{\pi\ell}{2} - i\sigma(\ell,\eta)}, \tag{10}$$

where $k = i\kappa$, $\eta_k = -i\eta$, and $\sigma(\ell, \eta)$ is the Coulomb phase shift. To discuss the limiting cases, is useful to introduce the complex turning point

$$z_t = -i\left(\eta + \sqrt{\eta^2 + \ell(\ell+1)}\right) \tag{11}$$

at which $d^2 H^+(\ell, \eta_k, z)/dz^2 = 0$.

According to the standard properties of the Coulomb wave functions [22, 23], one obtains the asymptotic expressions:

$$W_{-\eta,\ell+1/2}(2\kappa r) \simeq \left(\frac{\kappa r}{2\eta}\right)^{1/4} \exp\left(\eta - \eta\ln(\eta) - 2\sqrt{2\eta\kappa r}\right) \quad \text{for } \kappa r \ll |z_t|\ ,\ \eta \to +\infty, \tag{12}$$

$$W_{-\eta,\ell+1/2}(2\kappa r) \simeq \exp\left(-\kappa r - \eta\ln(2\kappa r)\right) \quad \text{for } \kappa r \gg |z_t|. \tag{13}$$

1. Near-threshold limit of SPANCs for charged particles

Let us first consider the limit (12) of $\eta \to +\infty$, which corresponds to very small separation energies. Since $\eta = \kappa_0/\kappa$, where $\kappa_0 = Z_b Z_c e^2\mu/\hbar^2$, the asymptotic part of the s.p. wave function near the particle emission threshold is

$$u_{\ell j}(r) \simeq \beta_{\ell j}\left(\frac{\kappa_0 r}{2\eta^2}\right)^{1/4} \exp\left(\eta - \eta\ln(\eta) - 2\sqrt{2\kappa_0 r}\right). \tag{14}$$

As the external norm (9) must be finite, and $\exp[\eta - \eta\ln(\eta)]/\eta^{1/2} \to 0$ for $\eta \to +\infty$, in the limit of very weak binding $\beta_{\ell j}$ must exhibit the universal $\eta-$dependence:

$$\tilde{\beta}_{\ell j}(\eta) = N_\beta(\ell, j)\eta^{1/2}\exp(\eta\ln\eta - \eta), \tag{15}$$

where $N_\beta(\ell, j)$ is a prefactor that depends on the structure of the s.p. state, in particular ℓ. To assess how quickly the limit (15) is reached, we performed calculations for the $1s_{1/2}$, $0p_{1/2}$, and $0d_{5/2}$ single-proton states in ^{17}F. The s.p. radial wave function $u_{\ell j}$ was calculated using the Woods-Saxon (WS) potential with the following parameters: the strength of the spin-orbit term $V_{\rm SO} = 3.68\,$MeV, radius $R_0 = 3.214\,$fm, and diffuseness $d = 0.58\,$fm. We took the Coulomb potential of a spherical uniform charge distribution with the radius R_0. For each ℓ, j, the depth of the central potential has been adjusted to the value of η. The value of $N_\beta(\ell, j)$ can be extracted from the calculated wave function at $\eta > 100$ and it is 10.786, 2.914, and 0.42 for the $1s_{1/2}$, $0p_{1/2}$, and $0d_{5/2}$ states, respectively. Figure 1 shows the $\eta-$dependence of the ratio $\beta_{\ell j}/\tilde{\beta}_{\ell j}$. The asymptotic behavior is reached at $\eta \approx 1$ for $\ell = 0$ and $\eta \approx 10$ for $\ell = 2$ and the ratio smoothly decreases with η suggesting a polynomial dependence on the proton separation energy (or a Maclaurin series in $1/\eta$). Guided by this result, we write:

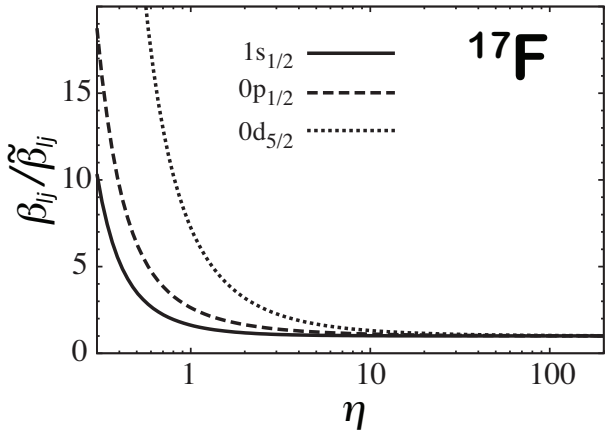

FIG. 1. The $\eta-$dependence of $\beta_{\ell j}/\tilde{\beta}_{\ell j}$ for $1s_{1/2}$, $0p_{1/2}$, and $0d_{5/2}$ s.p. proton wave functions in ^{17}F.

$$\beta_{n\ell j}(\eta) = \eta^{1/2}\exp(\eta\ln\eta - \eta)\sum_{i=0}^{\infty}\frac{a_i(n,\ell,j)}{\eta^i}. \tag{16}$$

It is worth noting that the term $\eta^{1/2}\exp(\eta\ln\eta - \eta)$, governing the rapid growth of SPANC around the threshold, is universal for *all charged particles* (proton, deuteron, α, ...), independent of their quantum state. The dependence on the structure is contained in the coefficients a_i of the Maclaurin series, which carry information on quantum numbers (n, ℓ, j) of the bound state. In the considered example of single-proton states in ^{17}F, the coefficients a_i were fitted in the range of proton separation energies $S_p^{(a)} < 10\,$MeV. An excellent fit has been obtained with the first five terms in the expansion (16). The resulting values a_i $(i = 0, \ldots, 4)$ are listed in Table I. To study the model dependence, for $1s_{1/2}$ we considered three values of WS diffuseness d. In this case, the coefficients a_i vary by 20-40% if d changes from the value of 0.46 fm to 0.7 fm. The variations in a_i with d are further reduced if the r.m.s. radius of the potential is kept constant while changing d. For instance, the changes in a_0 are $\sim 1\%$ in the calculations constrained in such a way.

TABLE I. Coefficients of the fourth-order Maclaurin series (16) fitted to the ratio $\beta_{\ell j}/\tilde{\beta}_{\ell j}$ of single-proton WS states in ^{17}F in the range of $S_p < 10$ MeV. For the $1s_{1/2}$ state, three values of diffuseness d (in fm) were used.

	$1s_{1/2}$			$0p_{1/2}$	$0d_{5/2}$
d	0.46	0.58	0.7	0.58	0.58
a_0	9.934	10.786	11.711	2.914	0.4200
a_1	0.8255	0.8889	0.9515	3.022	1.185
a_2	5.483	6.393	7.444	1.416	1.273
a_3	−0.9821	−1.157	−1.362	0.1411	−0.0408
a_4	0.4598	0.5635	0.6945	0.1676	0.2035

2. Large binding energy limit of SPANCs for charged particles

Now we consider the limit (13) of smaller η, which corresponds to finite separation energies that are small enough so that the η-variations of $\mathcal{N}_{\rm int}$ can be neglected.

In this case, the asymptotic part of the wave function shows the usual exponential decay:

$$u_{\ell j}(r) \simeq \beta_{\ell j} \exp\left(-\kappa_0 r/\eta - \eta \ln(2\kappa_0 r/\eta)\right). \quad (17)$$

In this case, in order to keep $\mathcal{N}_{\rm ext}$ finite, $\beta_{\ell j}$ has to increase when η decreases. Consequently, when inspecting $\beta_{\ell j}$ as a function of η one can expect a minimum when η changes from small values toward the threshold ($\eta = +\infty$).

3. *Separation energy dependence of SPANCs for bound proton wave functions*

We shall now discuss the behavior of $\beta_{\ell,j}$ in the full energy range. Figure 2 shows $\beta_{\ell j}(\eta)$ for the p + ^{16}O

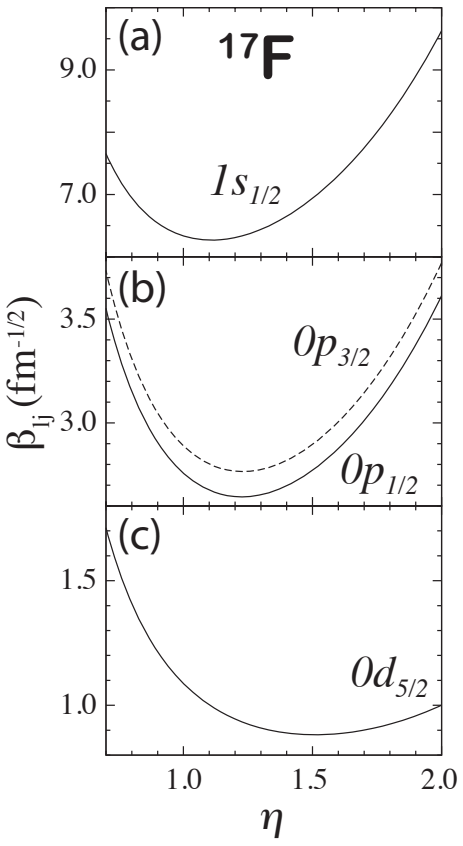

FIG. 2. Energy dependence of $\beta_{\ell j}$ for the bound-state proton s.p. wave functions in ^{17}F with $1s_{1/2}$ (a); $0p_{1/2}$ and $0p_{3/2}$ (b); and $0d_{5/2}$ (c).

capture reaction at $E_{\rm CM} = 0$ in channels where the proton has a relative angular momentum $\ell = 0$ ($1s_{1/2}$), $\ell = 1$ ($0p_{1/2}$ and $0p_{3/2}$), or $\ell = 2$ ($0d_{5/2}$). We used the same WS potential as in Sec. II A 1. It is seen that the behavior of SPANC as a function of η follows general considerations of Sec. II A 2. Namely, with increasing η, $\beta_{\ell,j}$ first decreases until a certain minimum value of $\eta = \eta_{\rm crit}$ is reached, and then increases again as the separation energy decreases towards the $S_p^{(a)} = 0$ threshold. We may thus conclude that $\eta_{\rm crit}$ separates the regimes of strong ($\eta < \eta_{\rm crit}$) and weak ($\eta > \eta_{\rm crit}$) binding for a given partial wave and Z_a. In general, $\eta_{\rm crit}$ scales approximately linearly with Z_b and it strongly depends on the angular momentum ℓ of the proton. On the other hand, the dependence on the channel angular momentum j is weak. The magnitude of $\beta_{\ell,j}$ decreases with ℓ. The case of $\ell = 0$ and large η (and $\beta_{\ell=0,j=1/2}$) shown in Fig. 2(a) is characteristic of a proton halo. However, as seen in Fig. 2 and discussed in Sec. II A 2, the large values of $\beta_{\ell,j}$ are also expected for very bound states, so a large SPANC is not an indicator of a proton halo.

The extreme regimes of SPANC can be characterized by the complex turning point z_t given by Eq. (11). The low-binding regime of $\beta_{\ell,j}$ is reached for $\kappa r \ll |z_t|$ and $\eta \to +\infty$. In this region, characterized by the condition

$$\left(\eta + \sqrt{\eta^2 + \ell(\ell+1)}\right)\eta \gg \kappa_0 R_f, \quad (18)$$

the proton wave function behaves asymptotically as $u_{\ell j}(r) \propto r^{1/4}\exp(-2\sqrt{2\kappa_0 r})$, i.e., its decay is slower than exponential. The strong-binding regime is reached at $\kappa r \gg |z_t|$, i.e.,

$$\left(\eta + \sqrt{\eta^2 + \ell(\ell+1)}\right)\eta \ll \kappa_0 R_f. \quad (19)$$

Here, the proton wave function shows the expected exponential decay (14).

4. *Near-threshold behavior of charged particle radiative capture cross sections*

Formally, one can discuss the charged particle radiative capture cross section in the two limits: (i) $\eta_{CM} \to \infty$ ($E_{\rm CM} \to 0$), and (ii) $\eta \to \infty$ ($S_c^{(a)} \to 0$), where $\eta_{CM} = Z_b Z_c e^2\sqrt{\mu/(2E_{CM})}/\hbar$. Whereas the CM energy of the system $\langle b + c\rangle$ can be varied experimentally, the charged particle separation energy is fixed for any state of the a-nucleus and, therefore, the limiting behavior of the radiative capture cross section when $\eta \to \infty$ cannot be studied experimentally in a single physical system. For a fixed value of η, the radiative capture cross-section $\sigma_{c\gamma}(\eta_{CM}, \eta)$ is exponentially reduced in the first limit ($\eta_{CM} \to \infty$) as:

$$\lim_{\eta_{CM}\to\infty} \sigma_{c\gamma} = \mathcal{S}_{bc}(\eta_{CM}, \eta)\frac{\exp(-2\pi\eta_{CM})}{E_{\rm CM}}. \quad (20)$$

As immediately follows from Eq. (8) and discussion in Sec. II A 1, in a sub-threshold regime ($\eta \to \infty$), the radiative capture cross-section $\sigma_{c\gamma}(\eta_{CM}, \eta)$ for a fixed value of η_{CM} diverges as:

$$\lim_{\eta\to\infty} \sigma_{c\gamma} \propto \mathcal{S}_{bc}(\eta_{CM}, \eta) \propto \eta\exp(2\eta\ln(\eta) - 2\eta). \quad (21)$$

The asymptotic behavior of $\sigma_{c\gamma}$ given by Eqs. (20) and (21) is expected for any charged particle radiative capture reaction.

5. Survey of proton SPANCs

To study the separation energy dependence, we calculated proton SPANCs using the WS potential with the radius $R_0 = 1.27\,A_c^{1/3}$ fm, diffuseness $d = 0.58$ fm, and spin-orbit strength $V_{\rm SO} = 4.0$ MeV; the Coulomb potential was taken as that of uniformly charged sphere distribution with the radius R_0. The WS depth was adjusted to the experimental separation energies $S_c^{(a)}$. Figures 3 and 4 survey the values of $\beta_{\ell,j}$ and η for the proton emission channels with $\ell = 1$ (p-shell) and $\ell = 2$ (sd-shell), respectively. The Z_a-dependence of $\eta_{\rm crit}$ is fairly weak in both cases. With the exception of the known proton halo ^{8}B, all other p-shell nuclei belong to the class $\eta < \eta_{\rm crit}$. The ground state of ^{12}N is found to have $\eta = \eta_{\rm crit}$. The neutron-rich nuclei have very small ground-state η-values; hence, their normalization constants $\beta_{\ell=1,j}(\eta)$ are large (see Fig. 2). An odd-even staggering of η – due to pairing – leads to an odd-even effect in $\beta_{\ell=1,j}(Z_a)$. The staggering in $\beta_{\ell j}$ is stronger for nuclei with $T_z \geq 0$ than in the proton-rich systems with $T_z < 0$.

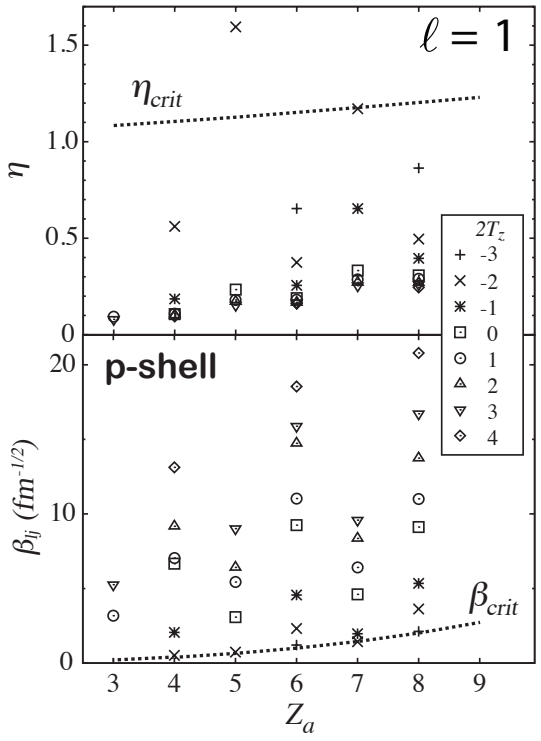

FIG. 3. Experimental values of η (top) and $\beta_{\ell,j}$ (bottom) for bound proton states with $\ell = 1$ and $j = 1/2, 3/2$ in various p-shell nuclei (Z_a, T_z). The curves of $\eta_{\rm crit}$ and $\beta_{\rm crit}$ are calculated for $T_z = -1/2$ nuclei. See text for details.

The data for sd-shell nuclei shown in Fig. 4 exhibit similar behavior. Most of the particle-stable sd-shell nuclei belong to the class $\eta < \eta_{\rm crit}$. The only system that falls decisively into the regime of weak binding is the $5/2^+$ ground state of ^{23}Al, which has a small separation energy of S_p=141 keV and a very large value of $\beta_{\ell,j}$ (see Ref. [24]

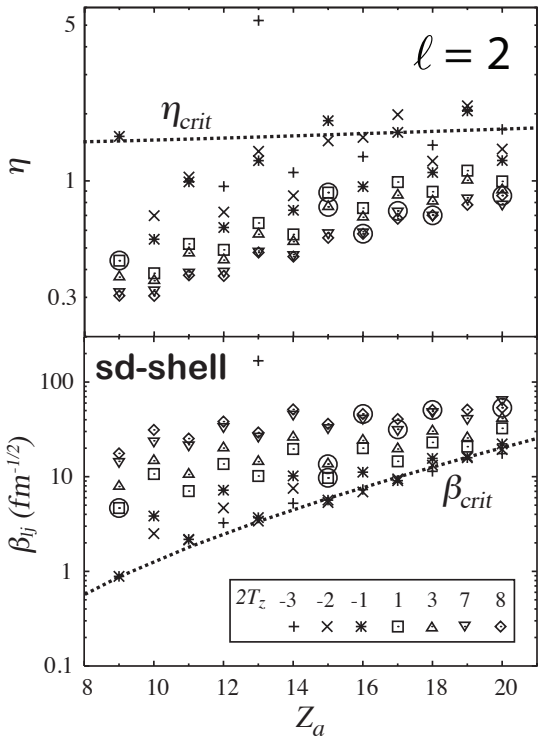

FIG. 4. Similar as in Fig. 3 except for $\ell = 2$ bound proton wave functions in sd-shell nuclei. For certain nuclei, the radiative proton capture with the channel angular momentum $j = 3/2, 5/2$ cannot populate the ground state of a nucleus a. In such cases (encircled symbols), we plot η and $\beta_{\ell,j}$ for the lowest-energy excited state that is populated by the capture with $\ell = 2$ protons.

for a recent discussion). Other nuclei with $\eta > \eta_{\rm crit}$ are ^{29}P, ^{32}Cl, and ^{36,37}K whereas ^{17}F, ^{30}S, ^{33}Cl, and ^{37}Ca are situated at the critical line $\eta_{\rm crit}(Z_a)$. A pronounced odd-even staggering of η and $\beta_{\ell,j}$ is seen for both proton-rich and neutron-rich systems. The values of SPANCs for proton-rich nuclei remain close to $\beta_{\rm crit}$.

The transition from $\eta < \eta_{\rm crit}$ to $\eta > \eta_{\rm crit}$ can be further explored by studying different particle-stable excited states in one nucleus, having different values of η, populated in the capture reaction. Figure 5(a) shows experimental values of η as a function of the proton separation energy for several excited states of ^{22}Mg. A transition from $\eta < \eta_{\rm crit}$ to $\eta > \eta_{\rm crit}$ takes place between the $J_i^\pi = 4_1^+$ and 2_2^+ levels. The corresponding SPANCs are displayed in Fig. 5(b). Those with $\ell = 2$ show a minimum at the 2_2^+ state and the same is seen in the $\ell = 0$ channel. (One may notice the absence of $\ell = 0$ data points for the 0_1^+ and 4_1^+ levels as these states cannot be populated by the $\ell = 0$ proton capture.)

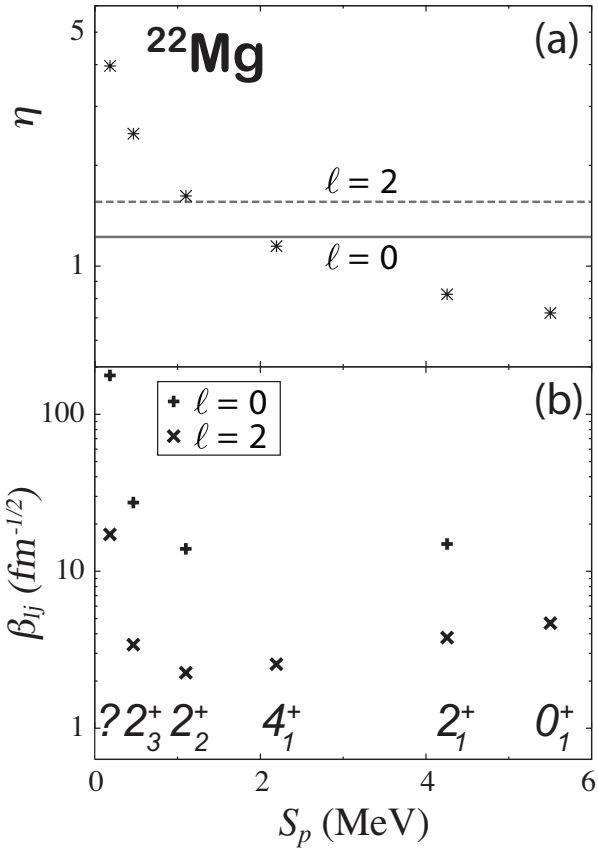

FIG. 5. Experimental values of η (a) and $\beta_{\ell,j}$ (b) for the low-energy states of ^{22}Mg as a function of the proton separation energy S_p. The values of $\eta_{\rm crit}$ in channels with $\ell = 0$ and $\ell = 2$ are indicated.

B. General properties of SPANCs for neutrons

The s.p. neutron wave function on the asymptotic region is

$$u_{\ell j}(r) \simeq \beta_{\ell j}\,(-i^{\ell})\;\kappa r\;h^{+}_{\ell}(i\kappa r), \tag{22}$$

where h^{+}_{ℓ} is the spherical Hankel function [22, 23]. In the limit of $\kappa \to 0$

$$(-i^{\ell})\;\kappa r\;h^{+}_{\ell}(i\kappa r) \simeq \frac{(2\ell-1)!!}{(\kappa r)^{\ell}} \quad \text{for } \ell \neq 0. \tag{23}$$

Using the same arguments as in Sec. II A 1, we conclude that close to the neutron threshold the neutron SPANC behaves as

$$\beta_{\ell j} \propto \kappa^{\ell} \quad \text{for } \ell \neq 0. \tag{24}$$

To discuss the special case of $\ell = 0$, we follow the analysis of Ref. [25]. The asymptotic part of the wave function for the s-wave is

$$u_{\ell j}(r) \simeq \beta_{\ell j} \exp(-\kappa r). \tag{25}$$

Since the external norm $\mathcal{N}_{\rm ext}$ (9) of (25) is finite, the near-threshold divergence of $\int_{R_f}^{+\infty} \exp(-2\kappa r)\,dr \propto \kappa^{-1}$ must be compensated by the κ-dependence of SPANC:

$$\beta_{\ell=0 j=1/2} \propto \sqrt{\kappa}. \tag{26}$$

In the limit of the large binding energy, the neutron wave function exhibits the exponential behavior:

$$u_{\ell j}(r) \simeq \beta_{\ell j} \exp(-\kappa r). \tag{27}$$

Using the reasoning of Sec. II A 2, we conclude that $\beta_{\ell j}$ has to increase with κ. Consequently, in the neutron case, $\beta_{\ell j}$ should monotonically decrease with κ all the way down to zero.

To describe $\beta_{\ell j}$ for neutrons in a wider energy range, one can employ the power series expansion in κ:

$$\beta_{\ell=0,1/2} = \sum_{i=0}^{\infty} a^{(i)}_{\ell=0,1/2}\kappa^{(i+1/2)} \quad \text{for } \ell = 0, \tag{28a}$$

$$\beta_{\ell,j} = \sum_{i=0}^{\infty} a^{(i)}_{\ell,j}\kappa^{(i+\ell)} \quad \text{for } \ell \neq 0. \tag{28b}$$

Figure 6 shows $\beta_{\ell j}$ for the bound $1s_{1/2}$, $0p_{1/2}$, and $0d_{5/2}$ neutron s.p. wave functions. The short-dashed lines are fits with two leading terms to expansions (28). In general, the coefficients $a^{(i)}_{\ell,j}$ in Eq. (28) depend on the choice of an average potential. The case $\ell = 0$ is special. Since $\mathcal{N}_{\rm ext} \to 1$ in the limit $S_n \to 0$, SPANC becomes potential-independent. In particular, the coefficient $a^{(0)}_{\ell=0,1/2}$ in Eq. (28) becomes $\sqrt{2}$ in the limit of zero binding.

For $\ell = 1, j = 1/2$, the values of $a^{(0)}_{\ell,j}$ are 1.549, 1.612, and 1.681 for d equal to 0.46 fm, 0.58 fm, 0.7 fm, respectively. Variations of $a^{(0)}_{\ell,j}$ with d become insignificant if the r.m.s. radius of the potential is kept constant.

III. CONTINUUM SHELL MODEL DESCRIPTION OF ANCS IN MIRROR SYSTEMS

An extensive analysis of proton and neutron ANCs for light mirror nuclei has been performed using SM and cluster model wave function and various effective NN interactions [1, 15–18]. It has been found that the ratio of proton and neutron ANCs for mirror nuclei,

$$\mathcal{R} = |C_p/C_n|^2, \tag{29}$$

is rather insensitive to model details and can be well approximated by the expression

$$\mathcal{R} \approx \mathcal{R}_0 \equiv \left| \frac{e^{i\sigma_\ell(-i\eta)} F_{\ell,-i\eta}(i\kappa_p R_f)}{\kappa_p R_f j_\ell(i\kappa_n R_f)} \right|^2, \tag{30}$$

where $\sigma_\ell(-i\eta)$ is the Coulomb phase shift associated with the imaginary momentum $i\kappa_p$, and $F_{\ell,-i\eta}$ and j_ℓ are the

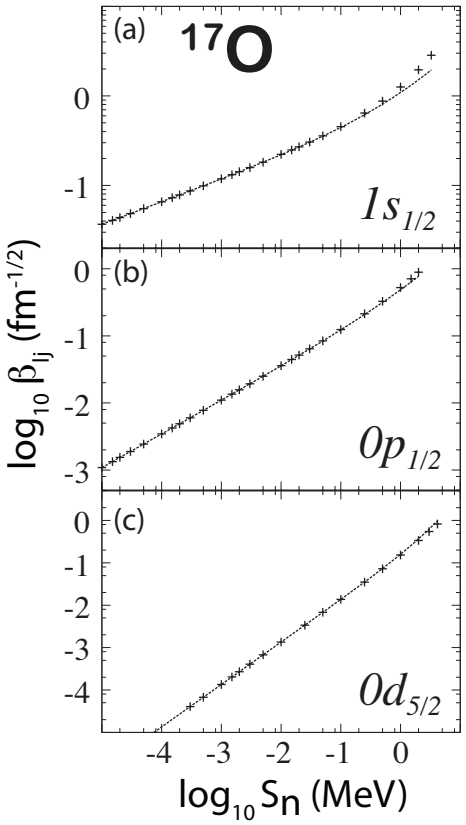

FIG. 6. $\beta_{\ell j}$ for the bound neutron states $1s_{1/2}$ (a), $0p_{1/2}$ (b), and $0d_{5/2}$ (c) in ^{17}O as a function of S_n. The fits using expansions (28) are shown by dotted lines. The same WS potential as in Fig. 1 was used.

regular Coulomb and regular Bessel functions, respectively. It is to be noted that our expression for $\mathcal{R}_0$ differs from that of Refs. [1, 16] because of different definitions of complex Coulomb wave functions. In our work we follow the convention of Refs. [26, 27], which results in the appearance of an additional factor $e^{i\sigma_\ell(-i\eta)}$ in Eq. (30). It should be noted that $\beta^2_{\ell j}$ for both protons and neutrons depends uniquely on the single-particle wave function $u_{\ell j}$ defined in Eq. (4) and, hence, is not affected by the continuum coupling.

We shall verify these findings in the CSM. As ANCs are impacted by the configuration mixing and continuum coupling through the spectroscopic amplitudes $S^{1/2}_{\ell j}$ (4), the OQS framework of the CSM is particularly well-suited for the description of the ANCs in mirror nuclei. Indeed, since the one-nucleon separation energies in mirror systems can be appreciably different, the particle continuum, both of a resonant and non-resonant character, can impact properties of states involved, especially when dealing with near-threshold energies.

The principal difficulty in the formulation of the CSM is the treatment of the unbound space of states, i.e., resonances and the non-resonant continuum [19, 20, 28]. Therefore, whatever strategy is adopted to formulate the configuration interaction approach for OQSs, the key points are: (i) the treatment of the s.p. continuum, and (ii) the definition of the many-body Fock space.

Historically, the first approach to formulate the CSM in Hilbert space was based on the projection technique [29]. Here, the Hilbert space is divided into orthogonal subspaces $\mathcal{Q}_{i_{\rm cont}}$ containing different numbers $i_{\rm cont}$ ($i_{\rm cont} = 0, 1, \cdots$) of particles in the scattering continuum. An OQS description of $\mathcal{Q}_0$ space includes couplings to the environment of decay channels through the energy-dependent effective Hamiltonian [30–32]:

$$\mathcal{H}_{\mathcal{Q}_0\mathcal{Q}_0}(E) = H_{\mathcal{Q}_0\mathcal{Q}_0} + W_{\mathcal{Q}_0\mathcal{Q}_0}(E), \qquad (31)$$

where $H_{\mathcal{Q}_0\mathcal{Q}_0}$ is the standard SM Hamiltonian describing the internal dynamics in the closed quantum system approximation and $W_{\mathcal{Q}_0\mathcal{Q}_0}(E)$ is the energy-dependent continuum coupling term. The Hamiltonian (31) is Hermitian below the first particle emission threshold and complex-symmetric above it.

The s.p. resonances have to be regularized before including them in the subspace of discrete states. An effective way of doing this is based on the anamneses of resonances, i.e., images of resonances in the space of $\mathcal{L}^2-$functions [33]. Bound s.p. states, resonance anamneses, and real-energy scattering continuum states form a complete s.p. basis [33]. The many-body Hilbert space can be represented by Slater determinants spanned by this basis. In practical applications of the real-energy CSMs, such as SMEC, one uses phenomenological arguments to restrict the number of particles in the scattering continuum. Technical difficulties associated with the correct treatment of the multiparticle channel wave functions rapidly grow with $i_{\rm cont}$; hence, in practical applications, the number of particles in the scattering continuum has so far not exceeded two [31].

Recently, a different strategy based on the rigged Hilbert space formulation of quantum mechanics [34] has resulted in the complex-energy CSM (the GSM) [35–37], which is a natural generalization of the standard SM for unbound systems. In this formulation, the maximum number of particles in the scattering continuum is not *a priori* prescribed, but follows from the Schrödinger variational principle for the many-body Hamiltonian. The s.p. GSM basis is given by the Berggren ensemble [38], which consists of Gamow (resonant) states and the non-resonant continuum. (For a detailed description of the GSM, see Ref. [20].) The GSM Hamiltonian is Hermitian. However, since the s.p. vectors have either outgoing or scattering asymptotics, the GSM Hamiltonian matrix is complex symmetric and its eigenvalues are complex above the particle emission threshold. Hence, both real-energy and complex-energy CSM formulations lead to a non-Hermitian eigenvalue problem above the threshold.

A. Theoretical framework

In both GSM and SMEC, we assume that the nucleus can be described as a system of $A_{val} = Z_{val}+N_{val}$ valence nucleons moving around a closed core $A_c = Z_c + N_c$.

1. GSM framework

The translationally invariant GSM Hamiltonian, written in intrinsic nucleon-core coordinates of the cluster-orbital shell model [39], can be written as:

$$H = \sum_{i=1}^{A_{val}} \left[\frac{p_i^2}{2\mu_i} + U_i \right] + \sum_{i<j}^{A_{val}} \left[V_{ij} + \frac{1}{M_c} \boldsymbol{p}_i \boldsymbol{p}_j \right], \quad (32)$$

where μ_i is the reduced mass of either the proton or neutron ($1/\mu_i = 1/m_i + 1/M_c$), U_i is the s.p. potential describing the field of the core, V_{ij} is the two-body residual interaction between valence nucleons, and the last term represents the two-body energy recoil. The particle-core interaction is a sum of nuclear and Coulomb terms:

$$U_i = U_i^N + U_i^C. \quad (33)$$

The nuclear potential U_i^N is approximated by a Woods-Saxon (WS) field with a spin-orbit term [35], and the Coulomb field U_i^C is generated by a Gaussian density of Z_c core protons [14]. Similarly, the residual interaction can split into nuclear and Coulomb parts:

$$V_{ij} = V_{ij}^N + V_{ij}^C, \quad (34)$$

where V^N is the modified surface Gaussian interaction (MSGI) [14] and V^C is the two-body Coulomb interaction that requires special treatment due to its infinite range [14, 40]. Namely, the Coulomb Hamiltonian V^C is rewritten as a sum of one-body Coulomb potential and two-body term:

$$\sum_{i<j}^{A_{val}} V_{ij}^C \rightarrow \sum_{i=1}^{A_{val}} U_{Z_{val}-1;\,i}^C + \sum_{i<j}^{A_{val}} \left[V_{ij}^C \right] - \sum_{i=1}^{A_{val}} \left[U_{Z_{val}-1;\,i}^C \right], \quad (35)$$

where $U_{Z_{val}-1;\,i}^C$ takes care of the long-range asymptotic behavior of the Coulomb interaction. As $U_{Z_c;\,i}^C + U_{Z_{val}-1;\,i}^C = U_{Z-1;\,i}^C$, the long-range physics of the Coulomb Hamiltonian is treated almost exactly. The two last terms in Eq. (35) and the two-body recoil term in Eq. (32) are expanded in a harmonic oscillator (HO) basis as their difference is short-ranged [14, 41]. In our calculations, we took nine HO shells with the oscillator length $b = 2\,\mathrm{fm}$ to carry out this expansion.

The radial overlap integrals were calculated using Eq. (2), where the sum over $\mathcal{B}$ states runs over the complete Berggren ensemble; hence, the result is independent of the s.p. basis representation. The ANC is obtained directly from Eq. (1).

The GSM calculations presented in this paper were carried out for p-shell systems ^{6}Li/^{7}Be ($\equiv^6$Li+$p \rightarrow ^7$Be), ^{6}Li/^{7}Li ($\equiv^6$Li+$n \rightarrow ^7$Li), and ^{7}Be/^{8}B, ^{7}Li/^{8}Li (assuming ^{4}He core), and sd-shell nuclei ^{16}O/^{17}F and ^{16}O/^{17}O (assuming ^{12}C core).

As the protons (neutrons) are well bound in ^{7}Be and ^{8}Li (^{7}Li and ^{8}B), only proton (neutron) bound s.p. shells are included in the model space, namely the $0p_{3/2}$ and $0p_{1/2}$ states. On the other hand, the full $p_{3/2}$ and $p_{1/2}$ Berggren basis, consisting of resonant and scattering states, is taken into account for the neutron (proton) space. In this way, completeness is assured in the neutron (proton) p-space. This is especially important for the ground state of the proton halo nucleus ^{8}B.

Since the precise description of reaction thresholds is crucial for precise determination of radial overlap integrals, the parameters defining the WS potential and MSGI interaction have been fitted independently for each pair of nuclei considered to reproduce the separation energy and lowest excited states of the heavier (parent) nucleus. The WS potential diffuseness has been assumed to be $d = 0.65\,\mathrm{fm}$ in all cases; WS radius has been set to $R_0 = 2\,\mathrm{fm}$ for $A = 6-8$ nuclei and $R_0 = 2.8\,\mathrm{fm}$ for $A = 16/17$ pairs; and spin-orbit strength was taken as 7.5 MeV for $A = 6-8$ nuclei, and 7.920 MeV (proton) and 8.463 MeV (neutron) for $A = 16/17$ pairs. For $A = 6/7$ pairs, the WS strength is 45.455 MeV for ^{6}Li/^{7}Be (protons) and ^{6}Li/^{7}Li (neutrons), and 55 MeV for ^{6}Li/^{7}Li (protons) and ^{6}Li/^{7}Be (neutrons). For $A = 7/8$ pairs, the corresponding values are 46.273 MeV (protons) and 65 MeV (neutrons) for ^{7}Be/^{8}B, and 75 MeV (protons) and 45.799 MeV (neutrons) for ^{7}Li/^{8}Li. For $A = 16/17$ pairs, the WS strength is 46.427 MeV and 46.034 MeV for protons and neutrons, respectively. The coupling strengths of MSGI depend on the quantum numbers J and T of the nucleon pair [14]. The $T = 0$ constants $V_{J,T=0}^N$ are listed in Table II and the $T = 1$ constants are given by $V_{J,T=1}^N = 0.5 V_{J,T=0}^N$.

TABLE II. Coupling constants $V_{J,T=0}^N$ of the MSGI residual interaction (in MeV fm^3) [14] for the considered pairs of nuclei and all allowed values of J. The J=4 and 5 coupling constants in $A = 16/17$ systems have been set to -9.0.

	$J=0$	$J=1$	$J=2$	$J=3$
^{6}Li/^{7}Be	−34.000	−23.200	−24.300	−17.384
^{6}Li/^{7}Li	−34.000	−23.200	−24.000	−17.000
^{7}Be/^{8}B	−25.593	−16.007	−10.288	−12.400
^{7}Li/^{8}Li	−24.662	−14.957	−10.592	−12.400
^{16}O/^{17}F	−16.540	−12.564	−5.870	−9.000
^{16}O/^{17}O	−16.540	−12.564	−5.870	−9.000

For $A = 16/17$ systems, the model space is the same for protons and neutrons: it consists of the resonant shells $0p_{1/2}$, $0d_{5/2}$, and $1s_{1/2}$, and the $s_{1/2}$ and $d_{5/2}$ scattering

continua. The $p_{1/2}$ and $d_{3/2}$ partial waves are discarded as they do not impact the asymptotic behavior of the 0^+_1 ground state of ^{16}O and the $5/2^+_1$ and $1/2^+_1$ states of ^{17}O and ^{17}F. In the pole approximation, in which only resonant states are considered, amplitudes of 2p-2h and 4p-4h $0p_{1/2} \to sd$ excitations are of the order of 10^{-3} and 10^{-6}, respectively. Consequently, as configuration mixing effects in the states considered are weak, only two particle-two hole excitations have been allowed from the proton and neutron $0p_{1/2}$ states, and only one particle has been allowed to occupy $s_{1/2}$ and $d_{5/2}$ scattering states. In all cases, scattering contours have been discretized utilizing a Gauss-Legendre quadrature. We have checked that a 45-point discretization for $A = 6/7$ (and 30-point discretization for other systems) is sufficient to maintain a correct asymptotic behavior of $I^a_{bc;\ell_j}(r)$ up to at least ~ 8 fm. For the s.p. basis, we took a Gamow Hartree-Fock (GHF) ensemble [37] corresponding to a parent nucleus. Sphericity of the GHF potential is guaranteed by the use of the uniform filling approximation. By taking the GHF basis we minimize configuration mixing. The many-body GSM states have been determined by a diagonalization of the GSM matrix using the Davidson method extended to complex-valued Hamiltonians. The identification of the outgoing GSM states has been carried out by applying the overlap method [36].

TABLE III. Calculated and experimental separation energies for the considered pairs of nuclei.

	$J^\pi(A-1)$	$J^\pi(A)$	$E_{\rm GSM}$ (MeV)	$E_{\rm exp}$ (MeV)
^{6}Li/^{7}Be	2^+	$3/2^-$	5.606	5.606
^{6}Li/^{7}Li	2^+	$3/2^-$	7.250	7.250
^{7}Be/^{8}B	$3/2^-$	2^+	0.137	0.137
^{7}Li/^{8}Li	$3/2^-$	2^+	2.034	2.033
^{16}O/^{17}F	0^+	$5/2^+$	0.601	0.600
^{16}O/^{17}O	0^+	$5/2^+$	4.143	4.143

The parameter optimization was carried out using the multidimensional Newton method. The fine-tuning was done manually to adjust the thresholds to experimental value with a 1 keV precision. For the excited states, we reproduce experimental data with a precision of a few tens of keV. The calculated separation energies are compared to experiment in Table III, while Table IV displays excitation energies and widths of the lowest excited states in the nuclei considered.

2. SMEC framework

In this study, the scattering environment is provided by one-nucleon decay channels, i.e. we solve the Schrödinger equation in the function space $\mathcal{Q}_0 \oplus \mathcal{Q}_1$. The SMEC solutions in $\mathcal{Q}_0$ are found by solving the eigenproblem

TABLE IV. Calculated and experimental excitation energies (in MeV) and widths (in keV) of the first excited states of the parent nucleus. The approximate width $\Gamma^{\rm (app)}_{\rm GSM}$ of Eq. (48) is shown for comparison.

	J^π	$E_{\rm GSM}$	$E_{\rm exp}$	$\Gamma_{\rm GSM}$	$\Gamma^{\rm (app)}_{GSM}$	$\Gamma_{\rm exp}$
^{7}Be	$1/2^-$	0.439	0.429	0	0	0
^{7}Li	$1/2^-$	0.459	0.478	0	0	0
^{8}B	1^+	0.771	0.770	24	23	36
^{8}B	3^+	2.278	2.320	275	258	350
^{8}Li	1^+	0.992	0.981	0	0	0
^{8}Li	3^+	2.222	2.255	21	21	32
^{17}F	$1/2^+$	0.495	0.495	0	0	0
^{17}O	$1/2^+$	0.870	0.871	0	0	0

for the non-Hermitian Hamiltonian (31):

$$\begin{aligned} \mathcal{H}_{\mathcal{Q}_0\mathcal{Q}_0}|\Psi_\alpha\rangle &= \mathcal{E}_\alpha(E,V_0)|\Psi_\alpha\rangle \\ \langle\Psi_{\bar\alpha}|\mathcal{H}_{\mathcal{Q}_0\mathcal{Q}_0} &= \mathcal{E}^*_\alpha(E,V_0)\langle\Psi_{\bar\alpha}| \end{aligned} \tag{36}$$

in the biorthogonal basis: $\langle\Psi_{\bar\alpha}|\Psi_\beta\rangle = \delta_{\alpha\beta}$. As usual, left $|\Psi_\alpha\rangle$ and right $|\Psi_{\bar\alpha}\rangle$ eigenvectors are related by the complex conjugation. In Eq. (36), E and V_0 stand for a scattering energy and a (real) continuum coupling constant in the coupling terms $H_{\mathcal{Q}_0,\mathcal{Q}_1}$ and $H_{\mathcal{Q}_1\mathcal{Q}_0}$:

$$W_{\mathcal{Q}_0\mathcal{Q}_0}(E) = H_{\mathcal{Q}_0\mathcal{Q}_1} G^{(+)}_{\mathcal{Q}_1}(E) H_{\mathcal{Q}_1\mathcal{Q}_0}, \tag{37}$$

where $G^{(+)}_{\mathcal{Q}_1}(E)$ is the one-nucleon Green's function. The energy scale is defined by the position of the one-nucleon emission threshold. At resonance, the eigenvalue of the effective Hamiltonian can be identified with the narrow pole of the scattering matrix (the S-matrix).

Inside of the interaction region, dominant contributions to the full solution of the Schrödinger equation in $\mathcal{Q}_0 \oplus \mathcal{Q}_1$ are given by the eigenfunctions of $\mathcal{H}_{\mathcal{Q}_0\mathcal{Q}_0}(E)$. This is the main reason why eigenfunctions of the non-Hermitian effective Hamiltonian are essential to understand properties of the OQS. The SMEC eigenvectors Ψ_α are related to the eigenstates Φ_j of the closed quantum system Hamiltonian $H_{\mathcal{Q}_0\mathcal{Q}_0}$ by a linear orthogonal transformation:

$$\Psi_\alpha = \sum_j b_{\alpha j}\Phi_j. \tag{38}$$

In our SMEC calculations, for the effective SM Hamiltonian $H_{\mathcal{Q}_0\mathcal{Q}_0}$ we took the Cohen-Kurath interaction [42] for valence nucleons outside the ^{4}He core for $A = 6-8$ systems. For *sd*-shell nuclei, we took the ZBM effective interaction [43] between valence nucleons outside the ^{12}C core. The continuum-coupling term (37) was approximated by means of the Wigner-Bartlett contact interaction:

$$V_{12} = V_0\left[\alpha + (1-\alpha)P^\sigma_{12}\right]\delta\left(\mathbf{r_1} - \mathbf{r_2}\right), \tag{39}$$

where P^{σ}_{12} is the spin exchange operator and $\alpha = 0.73$. The magnitude of the continuum coupling varies depending on the structure of SM wave function in a target nucleus with $(A-1)$ nucleons and the energy of the lowest one-nucleon emission threshold, which is fixed at the experimental value in all calculations. SMEC is particularly suited for studies of the qualitative effects of the continuum coupling because the strength of this coupling can be changed continuously from a SM limit ($V_0 = 0$) to physically relevant values. One should stress here that increasing V_0 lowers all the eigenvalues $\mathcal{E}_\alpha(E, V_0)$ in (36). The lowest eigenvalue describes the ground state (g.s.) of a system. For each value of V_0 we solve a fixed point equation $\mathcal{E}_\alpha(E, V_0) = E$ with experimental value of $E = -S_c^{(a)}$. Similar procedure applies to excited states.

The expectation value of any operator $\hat{O}$ can be calculated as:

$$\langle \hat{O} \rangle = \langle \Psi_{\bar{\alpha}} | \hat{O} | \Psi_\alpha \rangle \quad , \tag{40}$$

In case of the spectroscopic factor one has:

$$\hat{O} = a^\dagger |t\rangle\langle t| a, \tag{41}$$

where $|t\rangle$ is the target state of the $(A-1)$-system. For a single SM configuration, the ANC is proportional to the square root of the spectroscopic factor (7). In SMEC, the spectroscopic factors depend on the total energy E of the system and exhibit characteristic near-threshold variations that depend on the transferred angular momentum. In the multichannel representation of a many-body system, the flux conservation imposes an intricate interdependence between various spectroscopic factors not only on E but also on the strength of the continuum coupling V_0. This salient dependence of the ANC on the continuum coupling strength is a quantal effect, beyond the generic features discussed in Sec. II.

In the case of multi-channel coupling, the squared norm (3) becomes

$$|C_\ell|^2 = \sum_j |\beta_{\ell j}|^2 \, S_{\ell j}. \tag{42}$$

The ratio of proton and neutron ANCs for mirror nuclei (29) can be directly computed by means of Eq. (42) applied to charged-particle and neutral-particle radiative capture reactions. The continuum coupling in this case influences solely the spectroscopic factor $S_{\ell j}$.

B. CSM description of ANCs for bound states

In this section, we discuss the ANCs corresponding to single-nucleon capture reactions between bound states. We first present our GSM results ($E_{CM} = 0$). The ANCs in GSM can be directly extracted from the calculated radial overlap integrals by fitting their tail to Whittaker functions at large values of r (=7-8 fm). We can use such a direct method of extraction because the asymptotic behavior of $I^a_{bc;\ell j}(r)$ is well controlled in GSM.

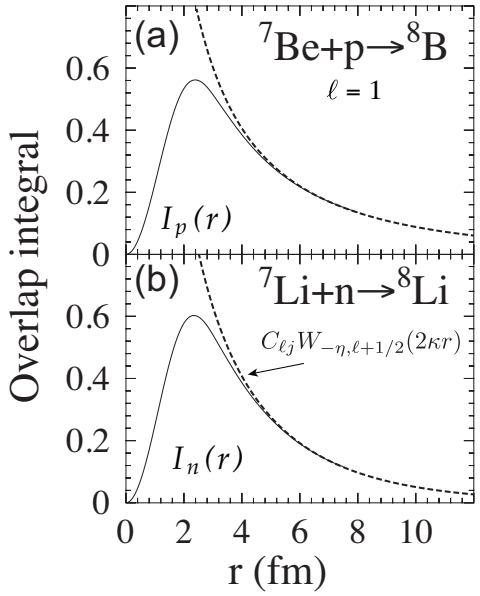

FIG. 7. Radial overlap integrals $I^a_{bc;\ell j}(r)$ calculated in GSM for $^7\mathrm{Be}_{3/2^-} + p \to {}^8\mathrm{B}_{2^+}$ (a) and $^7\mathrm{Li}_{3/2^-} + n \to {}^8\mathrm{Li}_{2^+}$ (b) for $\ell = 1$ and $j = 3/2$. The tail of the radial overlap integral is fitted by the Whittaker function (dashed line) to extract ANC.

Figure 7 shows how this procedure works for the radial overlap integrals corresponding to $\ell = 1$ ($0p_{1/2}$ and $0p_{3/2}$) protons and neutrons in the 2^+ ground states of the mirror nuclei ^{8}B, ^{8}Li. This example is non trivial as the configuration mixing is appreciable, and the g.s. of ^8B is a proton halo – as seen from the extended tail of the overlap function in Fig. 7(a).

The second example presented in Fig. 8 pertains to the first excited $J^\pi = 1/2^+_1$ subthreshold halo state in ^{17}F and ^{17}O, as seen in Table IV. Here, both proton and neutron overlap functions are very extended. Nevertheless, the extraction of the ANCs does not cause any problems.

The GSM predictions for ANC are listed in Table V together with the Variational Monte Carlo (VMC) results of Ref. [6] and experimental data. (See Ref. [48] for Greens function Monte-Carlo calculations for ^{7}Be and ^{7}Li.) One can see that the values of ANC for the $p_{1/2}$ proton and neutron partial waves are very different in GSM and VMC. While VMC values of ANCs in p-shell nuclei are usually closer to experiment for individual partial waves, both GSM and VMC perform well when the norm (3) is considered. The GSM results for the $5/2^+$ partial wave in the $A = 16 \to 17$ capture are very close to the data. This does not come as a surprise as the associated spectroscopic factors are almost equal to one, i.e., the ANC and SPANC values are practically identical.

The ratios $\mathcal{R}$ (29) predicted in GSM and VMC are displayed in Table VI. They are compared to experimental data and the approximate expression $\mathcal{R}_0$ of Eq. (30). (The predictions of microscopic cluster models can be

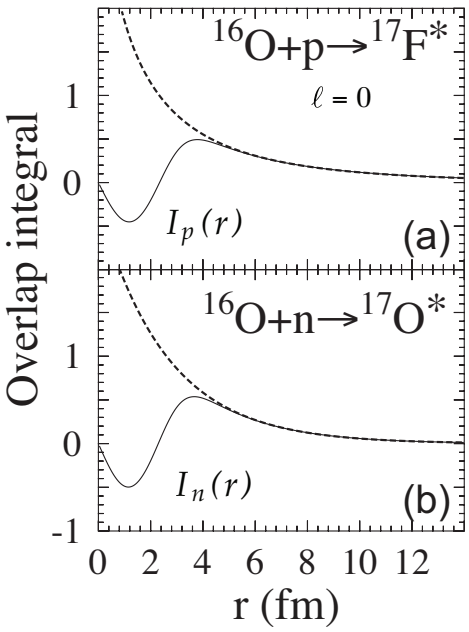

FIG. 8. Similar as in Fig. 7 but for $^{16}\mathrm{O}_{0^+} + p \to {}^{17}\mathrm{F}^*_{1/2^+}$ (a) and $^{16}\mathrm{O}_{0^+} + n \to {}^{17}\mathrm{O}^*_{1/2^+}$ (b) for $\ell = 0$.

found in Refs. [1] and [18].) As discussed in Ref. [1], as compared to ANCs, values of $\mathcal{R}$ exhibit less model dependence. Overall, predicted ratios $\mathcal{R}$ are fairly close to the estimate $\mathcal{R}_0$ and experiment.

In the following, we shall discuss the mirror ANCs using SMEC. The advantage of the projection technique used in SMEC is that the continuum coupling can be switched off and, therefore, the effect of the environment of decay channels on the mirror ANCs can be studied separately from the effect of internal dynamics governed by the effective interaction. The SMEC calculations presented in this paper were carried out for *p*- and *sd*-shell bound-state mirror reactions: ^{6}Li/^{7}Be and ^{6}Li/^{7}Li; ^{7}Be/^{8}B and ^{7}Li/^{8}Li; ^{11}C/^{12}N and ^{11}B/^{12}B; ^{16}O/^{17}F and ^{16}O/^{17}O; and ^{17}F/^{18}Ne and ^{17}O/^{18}O.

Table VII contains the summary of SMEC predictions for ANCs in *p*- and *sd*-shell mirror nuclei. To illustrate the impact of continuum coupling, we varied the continuum coupling strength V_0 in the physically relevant range from 0 (the SM limit) to -1.30 GeV fm^3. The resulting ratios $\mathcal{R}$ are listed in Table VIII.

It is seen that the dependence of ANCs and $\mathcal{R}$ on the continuum coupling is usually very weak. Indeed, in most considered cases the effect of the continuum coupling on ANCs does not exceed a few percent, and it is even smaller –a few per mil – for $\mathcal{R}$. It is instructive to compare ANCs of Tables V and VII, and the ratios $\mathcal{R}$ of Tables VI and VIII for the mirror pairs $(^7\mathrm{Be}/^7\mathrm{Li})_{3/2^-}$, $(^8\mathrm{Be}/^8\mathrm{Li})_{2^+}$, and $(^{17}\mathrm{F}/^{17}\mathrm{O})_{j^\pi}$. The GSM and SMEC results are extremely consistent when it comes to the the total ANCs (42) and their ratios.

As will be shown below, the effect of the continuum mixing depends on the distribution of spectroscopic factors in SM states coupled to the decay channel. This distribution is shown in Fig. 9 for selected examples discussed in this section.

A typical example, illustrated in Fig. 10, shows the variation of ANCs with V_0 for the mirror pair $(^7\mathrm{Be}/^7\mathrm{Li})_{3/2^-}$ and the mirror vertices: $^6\mathrm{Li}_{1^+} + \mathrm{p} \to {}^7\mathrm{Be}_{3/2^-} + \gamma$ and $^6\mathrm{Li}_{1^+} + \mathrm{n} \to {}^7\mathrm{Li}_{3/2^-} + \gamma$. The change of $C_{n\ell_j}$ with V_0 is due to the mixing of different $3/2^-$ SM states caused by the continuum coupling. This external mixing of SM states changes the spectroscopic amplitudes $S^{1/2}_{p_{1/2}}$ and $S^{1/2}_{p_{3/2}}$ in $C_{p_{1/2}}$ and $C_{p_{3/2}}$ ANCs, re-

TABLE V. GSM predictions for ANCs (in fm$^{-1/2}$) in mirror systems compared to VMC results [6] and experimental data [1, 44–47]. For $^6\mathrm{Li}_{1^+} + n \to {}^7\mathrm{Li}_{3/2^-}$, two experimental values have been reported [44]. For $A = 6 - 8$ systems, we show individual contributions from $p_{1/2}$ and $p_{3/2}$ channels and their Hermitian norm (3).

Overlap	j^π	GSM	VMC	Exp.
$^6\mathrm{Li}_{1^+} \xrightarrow{p} {}^7\mathrm{Be}_{3/2^-}$	$1/2^-$	0.431	1.870	—
	$3/2^-$	1.499	2.150	—
	$1/2^- + 3/2^-$	1.559	2.850	—
$^6\mathrm{Li}_{1^+} \xrightarrow{n} {}^7\mathrm{Li}_{3/2^-}$	$1/2^-$	0.422	1.652	—
	$3/2^-$	1.456	1.890	—
	$1/2^- + 3/2^-$	1.516	2.510	1.86 ± 0.06 2.57 ± 0.06
$^7\mathrm{Be}_{3/2^-} \xrightarrow{p} {}^8\mathrm{B}_{2^+}$	$1/2^-$	0.049	0.246	0.23 ± 0.01
	$3/2^-$	0.765	0.691	0.64 ± 0.03
	$1/2^- + 3/2^-$	0.767	0.733	0.68 ± 0.04
$^7\mathrm{Li}_{3/2^-} \xrightarrow{n} {}^8\mathrm{Li}_{2^+}$	$1/2^-$	0.041	0.218	0.22 ± 0.01
	$3/2^-$	0.750	0.618	0.62 ± 0.03
	$1/2^- + 3/2^-$	0.752	0.655	0.66 ± 0.03
$^{16}\mathrm{O}_{0^+} \xrightarrow{p} {}^{17}\mathrm{F}_{j^\pi}$	$5/2^+$	0.880	—	0.95 ± 0.09
	$1/2^+$	73.74	—	—
$^{16}\mathrm{O}_{0^+} \xrightarrow{n} {}^{17}\mathrm{O}_{j^\pi}$	$5/2^+$	0.805	—	0.82 ± 0.01
	$1/2^+$	2.785	—	—

TABLE VI. Ratio $\mathcal{R}$ (29) calculated in GSM and VMC [6], compared with estimate $\mathcal{R}_0$ (30) and experiment for the mirror systems of Table V.

Mirror pair	j^π	$\mathcal{R}_{\mathrm{GSM}}$	$\mathcal{R}_{\mathrm{VMC}}$	$\mathcal{R}_0$	$\mathcal{R}_{\mathrm{Exp.}}$
$(^7\mathrm{Be}/^7\mathrm{Li})_{3/2^-}$	$1/2^-$	1.04	1.28	1.06	—
	$3/2^-$	1.06	1.29	1.06	—
	$1/2^- + 3/2^-$	1.06	1.29	1.06	—
$(^8\mathrm{Be}/^8\mathrm{Li})_{2^+}$	$1/2^-$	1.39	1.27	1.12	1.08 ± 0.18
	$3/2^-$	1.04	1.25	1.12	1.08 ± 0.15
	$1/2^- + 3/2^-$	1.04	1.25	1.12	1.08 ± 0.15
$(^{17}\mathrm{F}/^{17}\mathrm{O})_{j^\pi}$	$5/2^+$	1.20	—	1.22	1.33 ± 0.20
	$1/2^+$	701	—	796	—

TABLE VII. SMEC predictions for ANCs (in $\mathrm{fm}^{-1/2}$) in mirror systems calculated with Cohen-Kurath ($A = 7, 8, 12$) and ZBM ($A = 17, 18$) interactions for three values of the continuum coupling strength V_0 (in GeV fm^3): 0 (SM limit), -0.65, and -1.30, all in the physically relevant range of continuum-coupling. Experimental binding energies were used.

Overlap	j^π	0 (SM)	0.65	1.30
$^6\mathrm{Li}_{1^+} \xrightarrow{p} {}^7\mathrm{Be}_{3/2^-}$	$1/2^-$	1.017	1.024	1.046
	$3/2^-$	1.279	1.282	1.291
	$1/2^-+3/2^-$	1.663	1.641	1.661
$^6\mathrm{Li}_{1^+} \xrightarrow{n} {}^7\mathrm{Li}_{3/2^-}$	$1/2^-$	0.988	0.995	1.016
	$3/2^-$	1.243	1.246	1.254
	$1/2^-+3/2^-$	1.588	1.595	1.614
$^7\mathrm{Be}_{3/2^-} \xrightarrow{p} {}^8\mathrm{B}_{2^+}$	$1/2^-$	0.164	0.149	0.088
	$3/2^-$	0.702	0.702	0.700
	$1/2^-+3/2^-$	0.721	0.717	0.705
$^7\mathrm{Li}_{3/2^-} \xrightarrow{n} {}^8\mathrm{Li}_{2^+}$	$1/2^-$	0.160	0.151	0.115
	$3/2^-$	0.685	0.685	0.684
	$1/2^-+3/2^-$	0.704	0.702	0.704
$^{11}\mathrm{C}_{3/2^-} \xrightarrow{p} {}^{12}\mathrm{N}_{1^+}$	$1/2^-$	1.122	1.126	1.127
	$3/2^-$	0.535	0.530	0.527
	$1/2^-+3/2^-$	1.242	1.244	1.244
$^{11}\mathrm{B}_{3/2^-} \xrightarrow{n} {}^{12}\mathrm{B}_{1^+}$	$1/2^-$	0.971	0.975	0.977
	$3/2^-$	0.465	0.459	0.454
	$1/2^-+3/2^-$	1.077	1.078	1.077
$^{16}\mathrm{O}_{0^+} \xrightarrow{p} {}^{17}\mathrm{F}_{j^\pi}$	$5/2^+$	0.869	0.867	0.863
	$1/2^+$	75.91	76.01	76.09
$^{16}\mathrm{O}_{0^+} \xrightarrow{n} {}^{17}\mathrm{O}_{j^\pi}$	$5/2^+$	0.788	0.787	0.783
	$1/2^+$	2.771	2.773	2.776
$^{17}\mathrm{F}_{5/2^+} \xrightarrow{p} {}^{18}\mathrm{Ne}_{2^+_1}$	$1/2^+$	4.500	4.610	4.961
	$5/2^+$	1.739	1.758	1.702
$^{17}\mathrm{O}_{5/2^+} \xrightarrow{n} {}^{18}\mathrm{O}_{2^+_1}$	$1/2^+$	2.801	2.796	2.794
	$5/2^+$	1.504	1.544	1.580
$^{17}\mathrm{F}_{5/2^+} \xrightarrow{p} {}^{18}\mathrm{Ne}_{2^+_2}$	$1/2^+$	13.36	13.92	12.36
	$5/2^+$	1.644	1.820	2.299
$^{17}\mathrm{O}_{5/2^+} \xrightarrow{p} {}^{18}\mathrm{O}_{2^+_2}$	$1/2^+$	2.492	2.674	2.774
	$5/2^+$	0.705	0.683	0.679

TABLE VIII. Ratio $\mathcal{R}$ (29) calculated in SMEC for the mirror systems of Table VII. Experimental binding energies were used.

Mirror pair	j^π	$\mathcal{R}_{\mathrm{SM}}$	$\mathcal{R}_{0.65}$	$\mathcal{R}_{1.30}$
$(^7\mathrm{Be}/^7\mathrm{Li})_{3/2^-}$	$1/2^-$	1.059	1.059	1.060
	$3/2^-$	1.058	1.058	1.059
	$1/2^-+3/2^-$	1.058	1.058	1.060
$(^8\mathrm{Be}/^8\mathrm{Li})_{2^+}$	$1/2^-$	1.055	0.974	0.584
	$3/2^-$	1.048	1.048	1.047
	$1/2^-+3/2^-$	1.049	1.045	1.034
$(^{12}\mathrm{N}/^{12}\mathrm{B})_{1^+}$	$1/2^-$	1.333	1.333	1.331
	$3/2^-$	1.323	1.333	1.347
	$1/2^-+3/2^-$	1.331	1.333	1.334
$(^{17}\mathrm{F}/^{17}\mathrm{O})_{j^\pi}$	$5/2^+$	1.216	1.215	1.213
	$1/2^+$	750.7	751.4	751.3
$(^{18}\mathrm{Ne}/^{18}\mathrm{O})_{2^+_1}$	$1/2^+$	2.580	2.719	3.153
	$5/2^+$	1.336	1.295	1.160
$(^{18}\mathrm{Ne}/^{18}\mathrm{O})_{2^+_2}$	$1/2^+$	28.74	27.10	19.85
	$5/2^+$	5.438	7.099	11.46

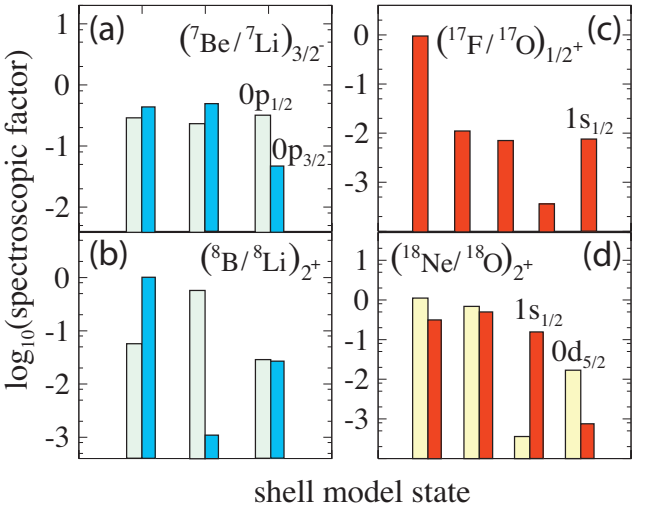

FIG. 9. (Color online) Distribution of spectroscopic strength for SM states coupled to the same decay channel in mirror pairs: $(^7\mathrm{Be}/^7\mathrm{Li})_{3/2^-}$ (a); $(^8\mathrm{B}/^8\mathrm{Li})_{2^+}$ (b); $(^{17}\mathrm{F}/^{17}\mathrm{O})_{1/2^+}$ (c); and $(^{18}\mathrm{Ne}/^{18}\mathrm{O})_{2^+}$ (d). The SM states considered are represented by bars.

spectively. As seen in Fig. 9(a), the spectroscopic factors $S_{0p_{1/2}}$ and $S_{0p_{3/2}}$ in $J^\pi = 3/2^-_i$ states ($i = 1, 2, 3$) have all comparable values. The continuum mixing in this case is small, on the order of 2% (see Table VII).

Table VIII shows that in spite of different proton and neutron separation energies in the mirror pair $(^7\mathrm{Be}/^7\mathrm{Li})_{3/2^-}$, the effect of the continuum coupling on the ratio $\mathcal{R}$ for the $1/2^-$, $3/2^-$ partial waves, and the squared norm (42) is exceedingly small.

We now consider the mirror pair $(^8\mathrm{B}/^8\mathrm{Li})_{2^+}$ – involving a proton halo ^{8}B – and the mirror vertices: $^7\mathrm{Be}_{3/2^-} + \mathrm{p} \to {}^8\mathrm{B}_{2^+} + \gamma$ and $^7\mathrm{Li}_{3/2^-} + \mathrm{n} \to {}^8\mathrm{Li}_{2^+} + \gamma$. The target nuclei have $J^\pi = 3/2^-$; hence, they can be coupled to the final 2^+ state through $p_{1/2}$ or $p_{3/2}$ waves. Figure 11 shows the corresponding ANCs. The effect of the continuum coupling is rather important for a small component $p_{1/2}$ and practically negligible in $p_{3/2}$. Notice also a rather strong – and different – dependence of $C_{p_{1/2}}$ on V_0 in mirror systems. This different response to the continuum-coupling can be traced back to a different distribution of SM spectroscopic factors in the three lowest 2^+ states; see Fig. 9(b). As the spectroscopic factor $S_{0p_{3/2}}$ of the 2^+_1 state is close to 1, the state 2^+_1 is aligned with the decay channel already at V_0=0 and

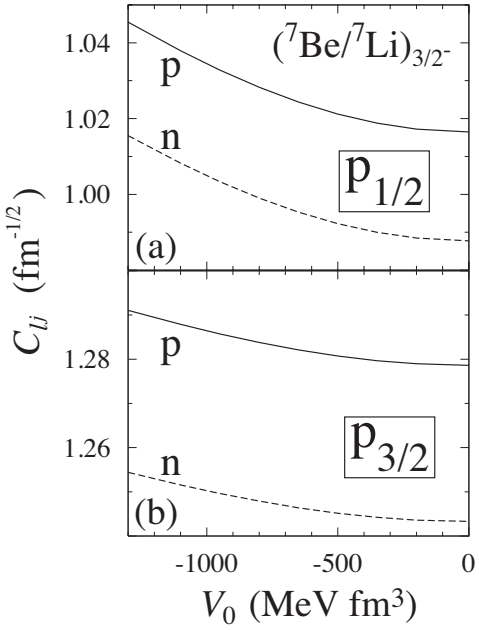

FIG. 10. ANCs for mirror nuclei $^7\mathrm{Be}_{3/2^-}$ (solid line) and $^7\mathrm{Li}_{3/2^-}$ (dashed line) calculated in SMEC as a function of the continuum-coupling strength V_0. Since the target nucleus ^{6}Li has $J^\pi = 1^+$, two partial waves are possible: $p_{1/2}$ (a) and $p_{3/2}$ (b).

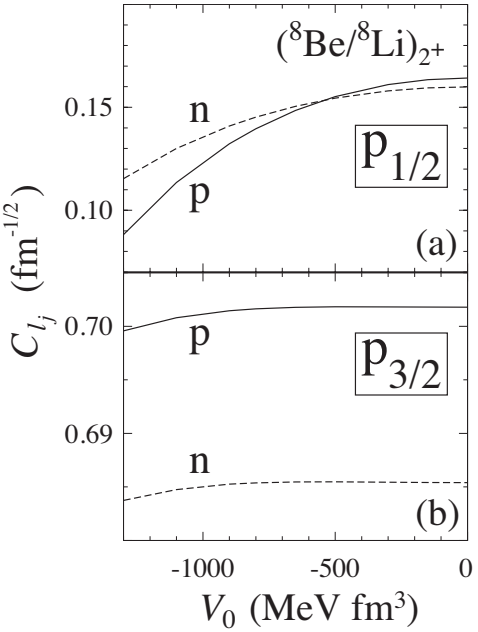

FIG. 11. Similar as in Fig. 10 but for mirror nuclei $^8\mathrm{B}_{2^+}$ (solid line) and $^8\mathrm{Li}_{2^+}$ (dashed line). Since the target $A = 7$ nucleus has $J^\pi = 3/2^-$, two partial waves are possible: $p_{1/2}$ (a) and $p_{3/2}$ (b).

no further redistribution of spectroscopic strength is possible through the continuum coupling. The situation is different for $S_{0p_{1/2}}$. In this case, the second 2^+ state has the largest spectroscopic factor and the external mixing leads to a redistribution of spectroscopic strength; hence, a change in ANC. The ratio of ANCs for the mirror pair (^{8}B/^{8}Li)$_{2^+}$ is shown in Table VIII. The variation of $\mathcal{R}$ with V_0 is of the order of 1 percent, and practically the whole effect is due to the $p_{1/2}$ wave.

As a third example, relevant in the context of GSM analysis, we shall consider the mirror pair (^{17}F/^{17}O) in $J^\pi = 5/2^+$ ground state and in the first excited proton halo state $1/2^+$. In the $J^\pi = 5/2^+$ ground state, both ^{17}F and ^{17}O couple to ^{16}O through the $d_{5/2}$ wave. The $0d_{5/2}$ spectroscopic strength is practically localized in the lowest $5/2^+$ state, i.e., the ground state is aligned with a decay channel. The same is true for the excited $1/2^+$ state, which practically exhausts the $1s_{1/2}$ spectroscopic strength, see Fig. 9(c). Consequently, as seen in Tables VII and VIII, the continuum coupling is negligible in the (^{17}F/^{17}O) case.

In the following, we shall discuss the mirror pair (^{18}Ne/^{18}O) in the two lowest 2^+ states, where the continuum coupling impacts ANCs significantly. In this case, the corresponding mirror vertices are: $^{17}\mathrm{F}^+_{5/2} + \mathrm{p} \rightarrow {}^{18}\mathrm{Ne}^+_{2_i} + \gamma$ and $^{17}\mathrm{O}^+_{5/2} + \mathrm{n} \rightarrow {}^{18}\mathrm{O}^+_{2_i} + \gamma$, where $i = 1, 2$. In ^{18}O, both 2^+ states are well bound, whereas in ^{18}Ne the state 2^+_2 is close to the proton threshold. It has been shown [49] that this state aligns strongly with the decay channel due to the continuum mixing of different 2^+ SM states.

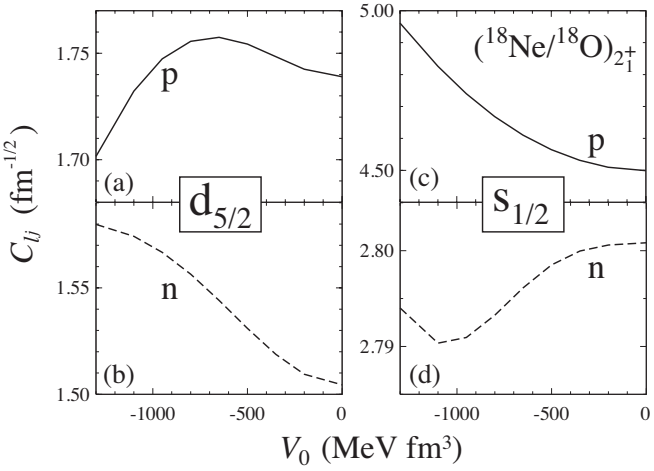

FIG. 12. Similar as in Fig. 10 but for mirror nuclei $^{18}\mathrm{Ne}_{2^+_1}$ (solid line) and $^{18}\mathrm{O}_{2^+_1}$ (dashed line). Since the target $A = 17$ nucleus has $J^\pi = 5/2^+$, two partial waves are possible: $d_{5/2}$ (left panels) and $s_{1/2}$ (right panels).

Figure 12 shows the mirror ANCs for $d_{5/2}$ and $s_{1/2}$ partial waves. It is interesting to notice that with increasing continuum coupling, $C_{d_{5/2}}$ first increases and then strongly decreases in ^{18}Ne, whereas it steadily increases in ^{18}O. As seen in Table VII, the overall variations in $C_{d_{5/2}}$ are $\sim 8\%$. Even stronger variations with V_0 are

seen for $C_{s_{1/2}}$. In the studied range of V_0 values, $C_{s_{1/2}}$ changes by almost $\sim 10\%$ in ^{18}Ne while it varies by $\sim 1\%$ in ^{18}O. A different behavior of $C_{d_{5/2}}$ and $C_{s_{1/2}}$ results in a particularly strong variation ($\sim 15\%$) of $\mathcal{R}$ for the 2^+_1 state; see Table VIII. This behavior can be attributed to the distribution of spectroscopic strength $0d_{5/2}$ ($1s_{1/2}$), which is primarily concentrated in the two (three) lowest 2^+ SM states.

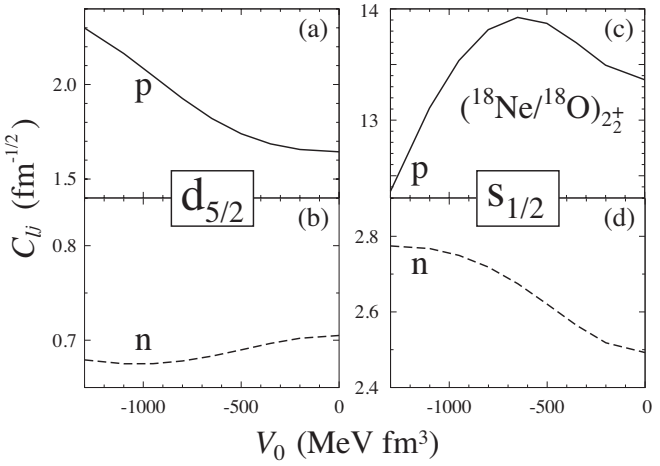

FIG. 13. Similar as in Fig. 12 but for $J^\pi = 2^+_2$ states in mirror nuclei.

Figure 13 shows the ANCs for $d_{5/2}$ and $s_{1/2}$ partial waves for the 2^+_2 state in ^{18}Ne and ^{18}O. Also in this case, ANCs are strongly affected by the continuum coupling: the ratio $\mathcal{R}$ changes by almost 50% in the considered range of V_0, as seen in Table VIII. The distribution of spectroscopic strength $0d_{5/2}$ ($1s_{1/2}$) in this case is concentrated in the two (three) lowest 2^+ SM states; see Fig. 9(d). It should be stressed that the large difference of mirror ANCs in ^{18}Ne and ^{18}O is due to the symmetry breaking in mirror spectroscopic factors and not due to the change of the ratio of $\beta^2_{\ell j}$ for protons and neutrons. A similar conclusion has been drawn in Ref. [50].

The realistic examples of SMEC calculations of ANCs presented in this section demonstrate that the distribution of spectroscopic strength over an ensemble of J^π SM states is crucial for determining the continuum coupling effect on ANCs. If the spectroscopic strength is strongly localized in one state, as in ^{17}F and ^{17}O, or very broadly distributed, as in ^{7}Be and ^{7}Li, then the corresponding ANC is fairly insensitive to the continuum coupling. On the other hand, if the spectroscopic strength is concentrated in several close-lying SM states, like in ^{18}Ne and ^{18}O, both mirror ANCs and their ratios may strongly depend on the coupling to the continuum – in particular if the state of interest lies close to the particle-emission threshold.

The distribution of spectroscopic strength strongly depends on the effective nucleon-nucleon interaction. In this sense, the quantitative effect of the continuum coupling on ANCs is strongly interaction-dependent. One should keep this in mind when making predictions about mirror reaction cross-sections. For a given model space and SM interaction, the relative importance of the continuum coupling on mirror ANCs can be *a priori* assessed by calculating spectroscopic amplitudes and their distribution in a standard SM. However, the effects of continuum coupling cannot be considered in an isolation from the optimization of the SM interaction to spectroscopic and reaction observables within a unified framework. By doing so, an inherent arbitrariness associated with predictions of ANCs can be reduced.

C. CSM description of ANCs for unbound states

The definition of ANCs via Eqs. (6,7) is no longer appropriate for negative separation energies, i.e., when the state of a nucleus a (A-particle system) is unbound with respect to the nucleus b ($A-1$-particle system). Indeed, in this case κ becomes complex and the Whittaker function becomes complex as well. The imaginary part of the Whittaker function is not vanishing even at the limit of vanishing width and the associated ANCs are complex.

1. *ANC of a complex-energy state and its relation to the particle width*

A suitable definition of the ANC for positive separation energies involves the outgoing Coulomb wave function $H^+_{\ell,\eta}(kr)$, where $k = (-2\mu S_a/\hbar^2)^{1/2}$ and $\eta = Z_b Z_c e^2 \mu/\hbar^2 k$:

$$I^a_{bc;\ell j}(r) \sim \frac{1}{r} C_{\ell j} H^+_{\ell,\eta}(kr). \tag{43}$$

Note that k and η are complex [12], as the state in A-particle systems is unbound. At the limit of vanishing width, k, $I^a_{bc;\ell j}$ and $H^+_{\ell,\eta}(kr)$ become real, so that $C_{\ell j}$ given by Eq. (43) becomes real as well.

For narrow resonances, ANCs can be related to the particle width [4]. However, the derivation of this relationship in Ref. [4] relies on the R-matrix theory – not used in the context of GSM – so it is useful to recall the derivation for the Gamow states. The overlap function $I^a_{bc;\ell j}(r)$ defined in Eq. (1) obeys a Schrödinger-like equation, albeit inhomogeneous [51]. However, separating the full interaction into a one-body term and a two-body residual interaction, the source term can be decomposed into a dominant homogeneous part and a residual inhomogeneous part, and the latter can be absorbed into the homogeneous part. This approximation has been tested successfully in Ref. [12] for both bound and unbound states. Moreover, as only narrow resonant states are involved, we will consider that the potential entering the equation defining $I^a_{bc;\ell j}(r)$ is real. This simplification breaks down for resonant states bearing a sizeable

width, for which complex potentials must be used [12], but is sound for narrow resonances.

Under these assumptions, one can easily derive the relation between ANC and partial width [52]. The function $\tilde{I}(r) \equiv rI^a_{bc;\ell j}(r)$ is a solution of the Schrödinger equation:

$$\tilde{I}''(r) = \left(\frac{\ell(\ell+1)}{r^2} + v(r) - k^2\right)\tilde{I}(r), \qquad (44)$$

where $v(r)$ is real and local. At large distances, the behavior of $\tilde{I}(r)$ is given by Eq. (43), and $\tilde{I}(r)$ is regular at origin: $\tilde{I}(r=0)=0$. The continuity equation for $\tilde{I}(r)$,

$$\tilde{I}^*(r)\tilde{I}'(r) - \tilde{I}'^*(r)\tilde{I}(r) = (k^{*2} - k^2)\int_0^r |\tilde{I}(s)|^2\, ds, \quad (45)$$

is obtained from Eq. (44) in the usual way by noting that

$$\tilde{I}^*(r)\tilde{I}''(r) - \tilde{I}''^*(r)\tilde{I}(r) = (k^{*2} - k^2)|\tilde{I}(r)|^2. \qquad (46)$$

By taking r in the asymptotic zone where (43) applies, noting that $k^{*2} - k^2$ is proportional to the partial width $\Gamma_{\ell j}$, and utilizing the standard mirror relation for Coulomb wave functions, $H^+_{\ell,\eta}(z)^* = H^-_{\ell,\eta^*}(z^*)$, one obtains:

$$\Gamma_{\ell j} = \frac{kH^-_{\ell,\eta^*}(k^*r)H^+_{\ell,\eta}(kr)' - k^*H^-_{\ell,\eta^*}(k^*r)'H^+_{\ell,\eta}(kr)}{2i\int_0^r |\tilde{I}(s)|^2\, ds} \times \frac{\hbar^2}{\mu}|C_{\ell j}|^2, \qquad (47)$$

where μ is the effective mass of the particle. To get rid of the explicit r-dependence in Eq. (47), further approximations are necessary [53]. Neglecting $\Im(k)$ in the Coulomb wave functions of the numerator of Eq. (47) implies that their Wronskian becomes equal to $2i\Re(k)$. Moreover, as $\tilde{I}(r)$ has a quasi-bound state character, it decreases exponentially along the real r-axis (unless r becomes extremely large, which we do not consider here), so that the integral in the denominator is almost equal to one when r is chosen in the asymptotic region. Under these assumptions, valid for narrow resonances, Eq. (47) simplifies to:

$$\Gamma_{\ell j} = \frac{\hbar^2}{\mu}|C_{\ell j}|^2\Re(k), \qquad (48)$$

which is the same expression as that obtained in Ref. [4], even though approximations and boundary conditions are different in the real-energy R-matrix approach and complex-energy Gamow-state formalism [53].

Expressing the total width Γ_ℓ in terms of the sum of partial widths $\Gamma_{\ell j}$ gives total ANC constant C_ℓ (3):

$$C_\ell = \sqrt{\sum_j |C_{\ell j}|^2} = \sqrt{\Gamma_\ell \frac{\mu}{\hbar^2\Re(k)}}. \qquad (49)$$

2. GSM description of ANCs for unbound states

Figure 14 compares radial overlap integrals (2) for the excited $J^\pi = 1^+_1$ states of ^{8}B and ^{8}Li in the $p_{3/2}$ channel. Since the 1^+_1 state of ^{8}B is a narrow one-proton resonance, the proton overlap integral acquires a small imaginary part. Figure 15 shows the radial overlap integrals for a 3^+_1 broad resonance in ^{8}B and a narrow mirror resonance in ^{8}Li. The tails of real and imaginary parts of radial overlap integrals are fitted with the outgoing Coulomb wave functions of a complex argument k. Table IX displays proton and neutron ANCs and their ratio $\mathcal{R}$ for the first excited $J^\pi_1 = 1^+_1$ state in ^{8}B and ^{8}Li.

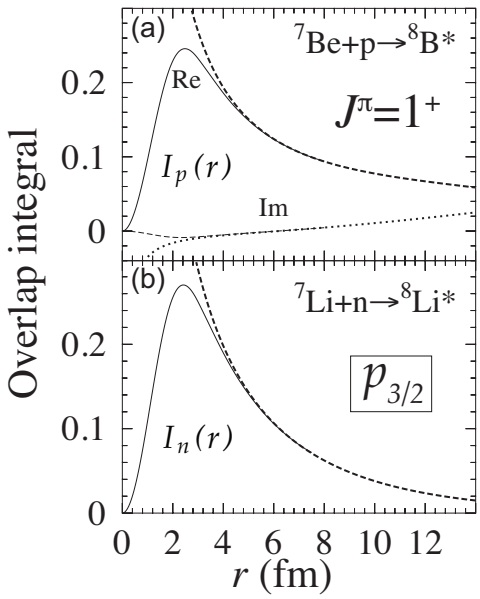

FIG. 14. Similar as in Fig. 7 but for $^7\mathrm{Be}_{3/2^-} + p \to {}^8\mathrm{B}_{1^+}$ (a) and $^7\mathrm{Li}_{3/2^-} + n \to {}^8\mathrm{Li}_{1^+}$ (b).

TABLE IX. Proton and neutron ANCs (in units of fm$^{-1/2}$), $\mathcal{R}_{\rm GSM}$ (29), and $\mathcal{R}_\Gamma$ (52) calculated in GSM for the $J^\pi = 1^+_1$ excited state in ^{8}B (one-proton resonance) and ^{8}Li. See text for details.

j^π	C_p	C_n	$\mathcal{R}_{\rm GSM}$	$\mathcal{R}_\Gamma$
$1/2^-$	$0.0322-i0.00138$	0.1379	0.0545	0.0021
$3/2^-$	$0.0442-i0.00273$	0.2090	0.0449	0.0018
$1/2^-+3/2^-$	0.0547	0.2504	0.0478	0.0019

3. SMEC description of ANCs for unbound states

To relate ANCs in bound-unbound mirror pairs and extract the proton decay width from the neutron ANC in

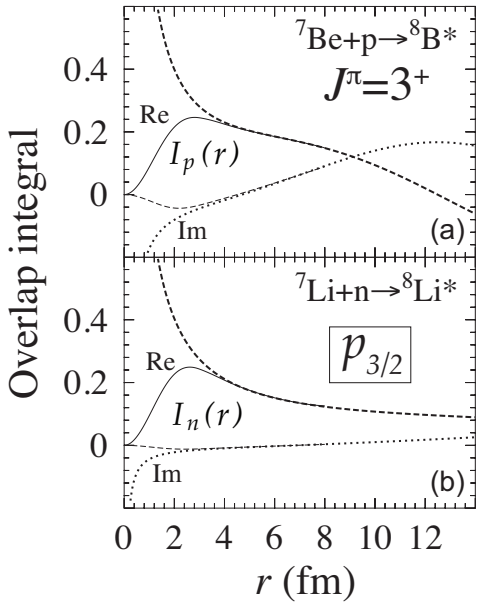

FIG. 15. Similar as in Fig. 14 but for the $J^\pi = 3^+_1$ resonance. In ^{8}B this state is a broad one-proton resonance which results in a large imaginary part of radial overlap integral.

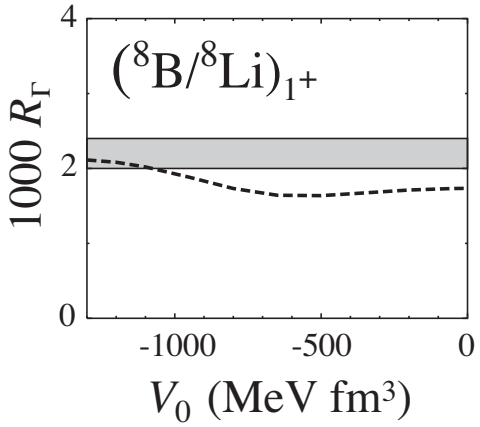

FIG. 16. The dependence of $\mathcal{R}_\Gamma$ (50) in SMEC on V_0 in mirror systems $^8\mathrm{B}(1^+_1)$ (proton resonance) and $^8\mathrm{Li}(1^+_1)$ (bound state). The shaded area shows the range of $\mathcal{R}_\Gamma$ extracted in Ref. [1] using experimental values of Γ_p [54] and C_n [45].

the bound mirror state, Timofeyuk *et al.* [1] introduced a quantity:

$$\mathcal{R}_\Gamma = \frac{1}{\hbar\, c}\,\frac{\Gamma_p}{|C_n|^2}, \tag{50}$$

where $|C_n|$ is given by Eq. (42) and Γ_p is the total width:

$$\Gamma_p = \sum_j \Gamma_{\ell j}\,|S_{\ell j}|\,, \tag{51}$$

where $\Gamma_{\ell j}$ is the partial proton width of a Gamow state with an quantum numbers ℓ and j. The modulus of a spectroscopic factor $S_{\ell j}$ is taken in order to ensure that Γ_p remains positive after the coupling to the particle continuum. For narrow resonances, using Eq. (48), one can express $\mathcal{R}_\Gamma$ in terms of proton and neutron ANCs:

$$\mathcal{R}_\Gamma = |C_p/C_n|^2\ \Re(k_p)\ \frac{\hbar c}{\mu_p c^2}. \tag{52}$$

As an example, let us consider the previously discussed case of the proton 1^+ resonance in ^{8}B and its bound mirror analog in ^{8}Li. Figure 16 shows the continuum coupling strength dependence of $\mathcal{R}_\Gamma$ computed with the approximate formula (51) using the spectroscopic factors obtained in SMEC. The shaded region correspond to the estimate of Ref. [1] based on experimental data for mirror states in ^{8}B and ^{8}Li. The SM prediction is $\mathcal{R}^{\rm SM}_\Gamma = 1.73\times10^{-3}$, whereas the experimental value extracted in Ref. [1] is $(2.2\pm0.2)\times10^{-3}$. The results of SMEC become compatible with the experiment for $V_0 < -1000$ MeV fm^3. The GSM prediction $\mathcal{R}_\Gamma = 1.88\times10^{-3}$ given in Table IX is fairly close to experiment and to SMEC.

The $p_{1/2}$ and $p_{3/2}$ neutron contributions to the ANC of $^8\mathrm{Li}_{1^+_1}$ are shown in Fig. 17. One can see that $p_{1/2}$ and $p_{3/2}$

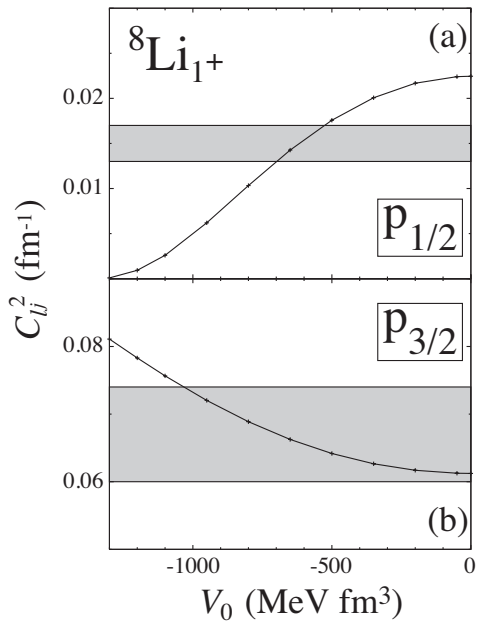

FIG. 17. Squared ANCs of the $p_{1/2}$ (a) and $p_{3/2}$ (b) neutron contributions to $^8\mathrm{Li}_{1^+_1}$. Shaded area mark experimental uncertainties on these quantities [1].

contributions have different dependence on V_0 which, in turn, reduces variations in $\mathcal{R}_\Gamma$. In general, for a physical range of V_0 in this mass region, -500 MeV fm$^3 > V_0 > -1200$ MeV fm^3, SMEC agrees somewhat better with experiment than SM.

IV. OUTLOOK

In the first part of the paper, we discussed the basic properties of ANCs and SPANCs. We broadly classified the behavior of SPANCs for charged and neutral particles in terms of the Sommerfeld parameter η and the wave number κ, respectively, as well as the orbital angular momentum. The extreme regimes of SPANC for charge particles can be characterized by the complex turning point z_t of the outgoing Coulomb wave function. We also discussed the near-threshold behavior of ANCs.

Based on the argument using the charge symmetry of the nuclear force, a simple relation (30) between proton and neutron ANCs in mirror pairs has been proposed [1]. The estimate $\mathcal{R}_0$ is very useful as it may help relating cross-sections of low-energy direct and resonance proton capture reactions, which are difficult or impossible to measure, with neutron ANCs obtained in reactions with stable beams. In the second part of this study, the link between mirror ANCs through relation (30) has been verified in our CSM calculations for different physical situations of the coupling to the scattering continuum and for various many-body states. It has been found that the key factor in determination of ANCs and the mirror ratio $\mathcal{R}$, as well as the sensitivity of ANCs to continuum coupling, is the distribution of spectroscopic strength that is both model- and interaction-dependent. For example, relative differences of $\mathcal{R}$ in GSM and VMC [6] can be as large as 30%, and the continuum coupling can change $\mathcal{R}$ by up to 50% in exceptional cases. Also, differences with respect to $\mathcal{R}_0$ can be non-negligible. In this sense, ANCs and their mirror ratios are interaction-dependent.

It has been found that the quantitative effect of the continuum coupling on ANCs and their ratios is minor if the spectroscopic strength is either localized in a single SM state or broadly distributed. This property is independent on binding energies of mirror states. On the other hand, if the spectroscopic strength is concentrated in several SM states, their coupling via the continuum space may result in a significant rearrangement of the spectroscopic strength; hence, appreciable variations of ANCs with respect to SM predictions. This effect is particularly strong for near-threshold states that align with the decay channel. Since these special cases can be *a priori* identified in standard SM calculations of the spectroscopic strength distribution, the qualitative effect of the continuum coupling on SM results for ANCs and their ratios can easily be assessed without resorting to sophisticated CSM calculations, which ultimately provide the quantitative answer.

Finally, let us state that uncertainties due to the model dependence can be significantly reduced if the effective SM interaction is optimized to both spectroscopic and reaction observables within a unified CSM framework. Work along these lines is in progress.

ACKNOWLEDGMENTS

Useful discussions with Filomena Nunes and Luke Titus are gratefully acknowledged. This work was supported by the Office of Nuclear Physics, U.S. Department of Energy under Contract Nos. DE-FG02-96ER40963 (University of Tennessee) and DE-FG02-10ER41700 (French-U.S. Theory Institute for Physics with Exotic Nuclei); by MSWiN Grant No. N N202 033837; by the CICYT-IN2P3 cooperation; and by the Academy of Finland and University of Jyväskylä within the FIDIPRO programme.

[1] N.K. Timofeyuk, R.C. Johnson, and A.M. Mukhamedzhanov, Phys. Rev. Lett. **91**, 232501 (2003); Phys. Rev. Lett. **97**, 069904(E) (2006).
N. K. Timofeyuk and P. Descouvemont, Phys. Rev. C **72**, 064324 (2005).

[2] L. D. Blokhintsev, I. Borbely, and Dolinsky, Part. Atom. Nucl. (ECHAYA) **8**, 1189 (1977).
M. Locher and T. Mizutani, Phys. Rep. C **46**, 43 (1978).
L. D. Blokhintsev, V. I. Kukulin, A. A. Sakharuk, D. A. Savin, and E. V. Kuznetsova, Phys. Rev. C **48**, 2390 (1993).

[3] H.M. Xu, C.A. Gagliardi, R.E. Tribble, A.M. Mukhamedzhanov, and N.K. Timofeyuk, Phys. Rev. Lett. **73**, 2027 (1994).

[4] C.A. Gagliardi, R.E. Tribble, J. Jiang, A.M. Mukhamedzhanov, L. Trache, H.M. Xu, S.J. Yenello, and X.G. Zhou, Nucl. Phys. A **588**, 327c (1995).
J.G. Ross, J. Gorres, C. Iliadis, S. Vouzoukas, M. Wiescher, R.B. Vogelaar, S. Utku, N.P.T. Batteman, and P.D. Parker, Phys. Rev. C **52**, 1681 (1995).
A. M. Mukhamedzhanov and R. E. Tribble, Phys. Rev. C **59**, 3418 (1999).

[5] A. Mukhamedzhanov, L. Blokhintsev, S. Brown, V. Burjan, S. Cherubini, V. Goldberg, M. Gulino, B. Irgaziev, E. Johnson, K. Kemper, et al., Nucl. Phys. A **787**, 321 (2007).

[6] K. Nollett and R. Wiringa, Phys. Rev. C **83**, 041001 (2011).

[7] A. M. Mukhamedzhanov and A. S. Kadyrov, Phys. Rev. C **82**, 051601 (2010).

[8] J.B. Ehrman, Phys. Rev. **81**, 412 (1951).
R.G. Thomas, Phys. Rev. **88**, 1109 (1952).

[9] J. Okołowicz, M. Płoszajczak, and Yan-an Luo, Acta Phys. Pol. **39**, 389 (2008).

[10] E.P. Wigner, Phys. Rev. **73**, 1002 (1948).

[11] G. Breit, Phys. Rev. **107**, 1612 (1957).

[12] N. Michel, W. Nazarewicz, and M. Płoszajczak, Nucl. Phys. A **794**, 29 (2007).

[13] N. Michel, W. Nazarewicz, and M. Płoszajczak, Phys. Rev. C **75**, 031301(R) (2007).

[14] N. Michel, W. Nazarewicz, and M. Płoszajczak, Phys. Rev. C **82**, 044315 (2010).

[15] N.K. Timofeyuk, Nucl. Phys. A **632**, 38 (1998).
N.K. Timofeyuk and S.B. Igamov, Nucl. Phys. A **713**, 217 (2003).

[16] N. K. Timofeyuk and P. Descouvemont, Phys. Rev. C **71**, 064305 (2005).

[17] N. K. Timofeyuk, P. Descouvemont, and R. C. Johnson, Phys. Rev. C **75**, 034302 (2007).

[18] L. J. Titus, P. Capel, and F. M. Nunes, Phys. Rev. C **84**, 035805 (2011).

[19] J. Okołowicz, M. Płoszajczak and I. Rotter, Phys. Reports **374**, 271 (2003).

[20] N. Michel, W. Nazarewicz, M. Płoszajczak, and T. Vertse, J. Phys. G: Nucl. Part. Phys. (Topical Review) **36**, 013101 (2008).

[21] A. M. Mukhamedzhanov and F. M. Nunes, Phys. Rev. C **72**, 017602 (2005).
D. Y. Pang, F. M. Nunes, and A. M. Mukhamedzhanov, Phys. Rev. C **75**, 024601 (2007).

[22] M. Abramowitz and I. Stegun, *Handbook of Mathematical Functions* (Dover Publications, Inc., New York, 1970).

[23] I. Gradshteyn and I. Ryzhik, *Table of Integrals, Series, and Products* (Academic, New York, 1980).

[24] A. Banu, L. Trache, F. Carstoiu, N. L. Achouri, A. Bonaccorso, W. N. Catford, M. Chartier, M. Dimmock, B. Fernández-Dominguez, M. Freer, et al., Phys. Rev. C **84**, 015803 (2011).

[25] K. Riisager, A.S. Jensen, and P. Møller, Nucl. Phys. A **548**, 393 (1992).

[26] I.J. Thomson and A.R. Barnett, J. Comp. Phys. **64**, 490 (1986).

[27] N. Michel, Comput. Phys. Commun. **176**, 232 (2007).

[28] N. Michel, W. Nazarewicz, Płoszajczak, and T. Vertse, J. Phys. G **36**, 013101 (2009).

[29] H. Feshbach, Ann. Phys. (NY) **5**, 357 (1958).
H. Feshbach, Ann. Phys. (NY) **19**, 287 (1962).

[30] H.W. Barz, I. Rotter and J. Höhn, Nucl. Phys. A **275**, 111 (1977).
I. Rotter, H.W. Barz, and J. Höhn, Nucl. Phys. A **297**, 237 (1978).

[31] K. Bennaceur, F. Nowacki, J. Okołowicz, and M. Płoszajczak, Nucl. Phys. A **651**, 289 (1999).
K. Bennaceur, F. Nowacki, J. Okołowicz, and M. Płoszajczak, Nucl. Phys. A **671**, 203 (2000).
J. Rotureau, J. Okołowicz, and M. Płoszajczak, Phys. Rev. Lett. **95**, 042503 (2005).
J. Rotureau, J. Okołowicz, and M. Płoszajczak, Nucl. Phys. A **767**, 13 (2006).

[32] A. Volya and V. Zelevinsky, Phys. Rev. Lett. **94**, 052501 (2005).
A. Volya and V. Zelevinsky, Phys. Rev. C **74**, 064314 (2006).

[33] J.B. Faes and M. Płoszajczak, Nucl. Phys. **A 800**, 21 (2008).

[34] I. Gel'fand and N. Vilenkin, *Generalized Functions*, vol. 4 (Academic Press, New York, 1961).
A. Bohm, *The Rigged Hilbert Space and Quantum Mechanics*, vol. 78 of *Lecture Notes in Physics* (Springer, New York, 1978).
G. Ludwig, *Foundations of Quantum Mechanics* (Springer, New York, 1983).

[35] N. Michel, W. Nazarewicz, M. Płoszajczak, and K. Bennaceur, Phys. Rev. Lett. **89**, 042502 (2002).
N. Michel, W. Nazarewicz, M. Płoszajczak, and J. Okołowicz, Phys. Rev. C **67**, 054311 (2003).
R. Id Betan, R. J. Liotta, N. Sandulescu, and T. Vertse, Phys. Rev. Lett. **89**, 042501 (2002).
J. Rotureau, N. Michel, W. Nazarewicz, M. Płoszajczak, and J. Dukelsky, Phys. Rev. Lett. **97**, 110603 (2006).
J. Rotureau, N. Michel, W. Nazarewicz, M. Płoszajczak, and J. Dukelsky, Phys. Rev. C **79**, 014304 (2009).

[36] N. Michel, W. Nazarewicz, M. Płoszajczak, and J. Okołowicz, Phys. Rev. C **67**, 054311 (2003).

[37] N. Michel, W. Nazarewicz, M. Płoszajczak, Phys. Rev. C, **70** 064313 (2004).

[38] T. Berggren, Nucl. Phys. **A 109**, 265 (1968).
T. Berggren and P. Lind, Phys. Rev. C **47**, 768 (1993).
P. Lind, Phys. Rev. C **47**, 1903 (1993).

[39] Y. Suzuki and K. Ikeda, Phys. Rev. C **38**, 410 (1988).

[40] N. Michel, Phys. Rev. C **83**, 034325 (2011).

[41] G. Hagen, M. Hjorth-Jensen, N. Michel, Phys. Rev. C **73**, 064307 (2006).

[42] S. Cohen and D. Kurath, Nucl. Phys. A **73**, 1 (1965).

[43] A.P. Zuker, B. Buck, and J.B. McGrory, Phys. Rev. Lett. **21**, 39 (1968).

[44] S.A. Goncharov, A.M. Mukhamedzhanov, E.A. Romanovsky, G.E. Valiev, I.R. Gulamov, T. Iskhakov, G. Nie, N.K. Tomopheyuk, R. Yarmukhamedov, V. Kroha *et al.*, Czech. J. Phys. **37**, 168 (1987).

[45] L. Trache, A. Azhari, F. Carstoiu, H. L. Clark, C. A. Gagliardi, Y.-W. Lui, A. M. Mukhamedzhanov, X. Tang, N. Timofeyuk, and R. E. Tribble, Phys. Rev. C **67**, 062801(R) (2003).

[46] G. Tabacaru, A. Azhari, J. Brinkley, V. Burjan, F. Carstoiu, C. Fu, C. A. Gagliardi, V. Kroha, A. M. Mukhamedzhanov, X. Tang, et al., Phys. Rev. C **73**, 025808 (2006).

[47] S. Burzynski, M. Baumgartner, H. Gubler, J. Jourdan, H. Meyer, G. Plattner, H. Roser, I. Sick, and K.-H. Möbius, Nucl. Phys. A **399**, 230 (1983).

[48] I. Brida, S. C. Pieper, and R. B. Wiringa, Phys. Rev. C **84**, 024319 (2011).

[49] R. Chatterjee, J. Okołowicz, M. Płoszajczak, Nucl. Phys. A **767**, 13 (2006).

[50] N. K. Timofeyuk and I. J. Thompson, Phys. Rev. C **78**, 054322 (2008).

[51] W.T. Pinkston and G.R. Satchler, Nucl. Phys. **72**, 641 (1965).

[52] J. Humblet and L. Rosenfeld,, Nucl. Phys. **26**, 529 (1961).

[53] B. Barmore, A.T. Kruppa, W. Nazarewicz, and T. Vertse, Phys. Rev. C **62** 054315 (2000).
A.T. Kruppa, and W. Nazarewicz, Phys. Rev. C **69**, 054311 (2004).

[54] F. Ajzenberg-Selove, Nucl. Phys. **A490**, 1 (1988).